Quaternary Science Reviews 344 (2024) 108969

Contents lists available at ScienceDirect

Quaternary Science Reviews

journal homepage: www.elsevier.com/locate/quascirev

Surges of the Black Rapids Glacier tracked climate over the last 600 years

D.H. Mann [a,*], P.R. Wilson [b], B.V. Gaglioti [c,d], P. Groves [e], M.E. Young [f]

[a] Institute of Arctic Biology, University of Alaska, Fairbanks, AK, 99709, USA
[b] Institute of Northern Engineering, University of Alaska, Fairbanks, AK, USA, 99775
[c] Water and Environmental Research Center, Institute of Northern Engineering, University of Alaska Fairbanks, Fairbanks, AK, USA, 99775
[d] Lamont-Doherty Earth Observatory at Columbia University, Palisades, New York USA, 10964
[e] Institute of Arctic Biology, University of Alaska, Fairbanks, AK, 99775, USA
[f] EA Engineering, Science, and Technology Inc., Sacramento, CA 95825, USA

ARTICLE INFO

Handling Editor: C. O'Cofaigh

ABSTRACT

Deposits of surge-type glaciers are widespread in the glacial geologic record; however, it is unclear how climate changes occurring at time scales of decades to centuries affect surge-type glaciers. Here we reconstruct the history of the Black Rapids Glacier (BRG) in the eastern Alaska Range since AD 1400 using a combination of geomorphology, stratigraphy, lichenometry, radiocarbon dating, and dendrochronology. Moraines in the glacier's foreland record four advances, all of which left deposits typical of surging glaciers. A surge in the AD 1600s dammed a lake which drained in an outburst flood ca. AD 1703-04. Another outburst flood from a larger glacier-dammed lake occurred in the AD 1400s. Based on the BRG's observed glaciology and its history over the last several centuries, its surge cycles have varied between 80 and 120 years. Between AD 1400 and 1900, the most extensive surges of the BRG coincided with minima in the Seuss / de Vries solar cycle when non-surging glaciers in the region also advanced. Synchroneity between the BRG, solar minima, and non-surging glaciers is surprising given that the terminus of the BRG was largely unresponsive to climate for 80–120 years between surges. One explanation is that the BRG's surge cycle shortened during the Little Ice Age (LIA, ca. AD 1300–1900) to the point that its climate-response lag resembled that of neighboring, non-surging glaciers. Although the reconstructed chronology of the BRG shows no indication of the surge cycle decreasing during the LIA, fading of the record with time makes it difficult to exclude this possibility. Another explanation is that the BRG's 80- to 120-year cycle is the result of tuning by the solar cycle over the course of millennia. Tuning occurred when quiescent phases that coincided with solar minima were shortened because of faster replenishment of the glacier's reservoir zone. The opposite occurred when the glacier's quiescent phases coincided with solar maxima. The net result was to align the surge cycle of the BRG with solar minima. Some combination of shortened surge cycles during the LIA and tuning by the solar cycle may be why the glacial-geologic record of this particular surge-type glacier provides a surprisingly dependable record of regional climate over the past 600 years.

1. Introduction

Surge-type glaciers are enigmatic end members of the global population of glaciers (Sevestre and Benn, 2015). While most glaciers track climate by maintaining a more or less steady flux of ice that balances accumulation with ablation, surging glaciers alternate between brief bouts of rapid flow and prolonged intervals of quiescence (Meir and Post, 1969; Jiskoot, 2011). In addition to the geological hazards that some of them pose (Haeberli and Drenkhan, 2022), surge-type glaciers are of interest because their dynamics provide insights into the instabilities and thresholds present within all glacier systems (Truffer et al., 2021). The internal processes that control glacial surging remain poorly understood (Raymond, 1987; Fowler, 1987; Harrison and Post, 2003; Benn et al., 2019). Understanding these processes is crucial for predicting the stability of present-day ice sheets and mountain glaciers as climate warms (Clarke et al., 1986).

Another reason surge-type glaciers are of interest is because they were widespread during the Pleistocene (Ingólfsson et al., 2016). Interpreting the geological records left by surging glaciers relies on understanding the processes governing their flow, the types of deposits they leave behind (Aradóttir et al., 2019), and how they respond to changing climate. The responses of surge-type glaciers to climate

* Corresponding author.
E-mail address: dhmann@alaska.edu (D.H. Mann).

https://doi.org/10.1016/j.quascirev.2024.108969
Received 1 June 2024; Received in revised form 3 September 2024; Accepted 12 September 2024

changes at varying time scales are complex and not well understood (Kochtitzky et al., 2020). This knowledge gap needs to be filled in order to interpret the deposits left by surge-type glaciers during prehistory.

Here we reconstruct the history of the Black Rapids Glacier (BRG) since ca. AD 1400. The BRG is one of the first surging glaciers documented in Alaska (Hance, 1937) and has been intensively studied by glaciologists since the 1970s (Heinrichs et al., 1996; Kienholz et al., 2017; Truffer et al., 2021). Our approach is multi-disciplinary and involves geomorphology, stratigraphy, lichenometry, radiocarbon dating, and dendrochronology. The goal is to reconstruct the chronology of recent surges and compare it to the timing of non-surging glaciers in the same region.

2. Background

2.1. Surge-type glaciers

A surge-type glacier episodically experiences sudden increases in ice velocity of up to two orders of magnitude (Meier and Post, 1969; Truffer et al., 2021). These episodes of rapid flow are often quasi-periodic (Striberger et al., 2011) and separated by longer intervals when the lower portions of the glacier stagnant and down-waste in place (Eisen et al., 2005). Surge-type glaciers are globally rare (<1% of all glaciers (Jiskoot et al., 2000)) but locally abundant (Sevestre and Benn, 2015). Numerous surging glaciers exist in the Alaska Range and eastern St. Elias Mountains (Post, 1960, 1969; Clarke et al., 1986; Herreid et al., 2016).

Surges represent the spectacular extremes of the multi-year variations in flow velocity occurring in many glaciers (Herreid and Truffer, 2016; Terleth et al., 2024). Various types of glaciers surge (Post, 1969), and two different types of surging glaciers are recognized depending on the surging process. Alaska-type surges are triggered by reorganization of the glacier's basal drainage system (hydraulic switching), while Svalbard-type surges are triggered by a change from cold-to warm-based conditions (thermal switching) (Jiskoot, 2011). The BRG appears to undergo classic, Alaska-type surges characterized by short-lived (1–2 years) surges followed by quiescent phases that last for decades to more than a century. In contrast, a Svalbard-type surging glacier undergoes a multi-year buildup to its surge phase, which lasts 3–10 years, followed by a quiescent phase lasting 50–500 years (Murray et al., 2003; Sevestre and Benn, 2015). Numerous intermediate types exist between the Alaska- and Svalbard type surging glaciers, and it is increasingly apparent that surging can result from a complex mixture of flow processes (Benn et al., 2022; Lovell et al., 2023).

Surge-type glaciers of all types have distinct morphometries and geographies. They tend to be larger, longer, and possess more tributary glaciers than non-surging glaciers in the same area (Clarke et al., 1986; Hamilton and Dowdeswell, 1996; Barrand and Murray, 2006; Lovell et al., 2023). A positive correlation between the occurrence of surge-type glaciers and active tectonic zones has been repeatedly suggested (Tarr and Martin, 1914; Amand, 1957), summarily dismissed (Post, 1960; 1967), and then reconsidered (Shugar et al., 2012). In the St. Elias Mountains, surge-type glaciers are most common where tectonic uplift is fastest (Clarke et al., 1986), and in the Alaska Range surge-type glaciers are concentrated along the Denali Fault (Post, 1969; Truffer et al., 2021).

2.2. Weather, climate, and glacial surging

Climate exerts a first-order control over the distribution of surge-type glaciers, with glacier geometry of secondary importance (Lovell et al., 2023). On a global basis, surge-type glaciers exist within a climate regime that is intermediate between the cold-dry and warm-moist extremes of where glaciers can exist (Sevestre and Benn, 2015).

The roles played by weather and climate in glacial surging relate to the mechanisms of surging. The presence of liquid water in the subglacial environment plays a key role in the rapid motion involved in the surge through its effects on basal shear stress (Raymond, 1987; Fowler, 1987; Kjær et al., 2006). Variations in weather and climate affect the temperature at the bed of the glacier and hence the amount of liquid water there, which can then affect the extent and rate of basal sliding (Harrison and Post, 2003). For example, subpolar (polythermal-based) glaciers in Svalbard typically move more slowly when surging than do warm-based glaciers surging at lower latitudes (Jiskoot, 2011). Warmer surface temperatures can also affect glacier motion by increasing the amount of meltwater routed to the glacier bed via crevasses where it can augment sliding (Sevestre et al., 2018).

Besides their effects on conditions at the glacier's bed, decadal-scale changes in climate also affect glacial surging by altering mass balance in the reservoir zone of the upper glacier (Truffer et al., 2021). The reservoir zone is the area in the upper reaches of a surge-type glacier that is deflated when ice is transferred rapidly down-glacier during a surge (Raymond, 1987). The glacier cannot surge again until this reservoir zone is replenished. Surge periodicity tends to be inversely correlated with ice-accumulation rate (Dowdeswell et al., 1991; Barrand and Murray, 2006; Kochtitzky et al., 2020; Sevestre and Benn, 2015). For example, the intervals between surges of the Variegated Glacier (Kamb et al., 1985) correlate with cumulative mass balance in its reservoir zone (Eisen et al., 2005).

Surge-type glaciers respond to changes in their surface mass balances in varying ways. An elegant record of glacial sedimentation in a lake fronting the Eyjabakkajökull in Iceland shows that its surge cycle shortened during the coldest periods of the Little Ice Age when the glacier's mass balances became more positive (Striberger et al., 2011). In contrast, the timing of surges of the Drangajökull ice cap, also in Iceland, show no clear relationship to climate over the past 300 years (Brynjólfsson et al., 2015). There is a suggestion that warming climate and declining mass balance have shortened the quiescent phase for the Lowell Glacier in the Yukon (Bevington and Copland, 2014). In contrast, despite reductions in surface mass balance since the 1930s, the Donjek Glacier has maintained a consistent surge interval, while the extent of its surges has decreased (Kochtitzky et al., 2020). In Svalbard (Svestre, 2015) and in Greenland (Lovell et al., 2023), warming temperatures have caused some surge-type glaciers to thin, changing thermal conditions at their beds from polythermal to cold-based and halting their surge cycles altogether. In contrast, Svestre et al. (2018) suggest that the surges of tidewater glaciers in Svalbard may become more frequent as climate warms and calving termini are destabilized.

At shorter, seasonal time scales, weather can influence when surges begin and end (Harrison and Post, 2003; Dunse et al., 2015; Solgaard et al., 2020). Surges typically start in winter and end in summer, and weather conditions can affect both the down-valley extent of a surge and when it ends (Eisen et al., 2005). For example, the most recent surges of the Donjek Glacier all began in years with particularly rainy summers (Kochtitzky et al., 2020). Short-term forcing by weather is most effective when the glacier is poised near its surge threshold (Jiskoot, 2011).

While climate and weather clearly influence glacial surging, the effects of century-scale climate changes on surging behavior remain unclear because of limited information on the long-term histories (>100 years) of surge-type glaciers, in particular for Alaska-type surging glaciers (Heinrichs et al., 1996; Kochtitzky et al., 2020). The contrasting responses of the surge-type glaciers in Iceland studied by Striberger et al. (2011) and by Brynjólfsson et al. (2015) mentioned above emphasize this point. Glaciers in the Alps that are known to have surged during the Little Ice Age (ca. AD 1300–1900) stopped surging in the 20th century (Hoinkes, 1969). Over the last 60 years in the Karakorum, glacial surging has increased in frequency, probably in response to increasing precipitation (Bhambri et al., 2017; Copland et al., 2011).

Multiple studies have reconstructed the histories of surge-type glaciers in Svalbard (Flink et al., 2015; Farnsworth et al., 2017; Lovell et al., 2018); however, the difficulty of obtaining high-resolution chronologies in Arctic settings and the fact that many of these glaciers terminated offshore make the resulting records best suited for millennial-scale

rather than decadal-scale comparisons with climate. Glacier surging became less frequent in Svalbard at the end of the Little Ice Age as thinning glaciers changed from a polythermal to a cold-based regime (Dowdeswell et al., 1995; Lovell et al., 2015). Over the last 15,000 years in Svalbard, glacier dynamics at times superseded climate drivers; at other times, surges coincided with periods of glaciogenic climate (Larsen et al. (2018). How decade-to-century changes in climate affect surging behavior remains a gap in our understanding of the surging-glacier phenomenon, and this gap has significant implications for understanding the dynamics of both modern and ancient glacial systems (Ingólfsson et al., 2016).

2.3. Glacial surging and glacial lake outburst floods (GLOFS)

The most obvious geological hazard posed by a surging glacier involves it overriding human infrastructure. Less obvious, but often more serious are the impacts of outburst floods from glacier-dammed lakes (Clague and O'Connor, 2021; Haeberli and Drenkhan, 2022; Lützow et al., 2023). Multiple mechanisms exist for glacial lake outburst floods (GLOFs). Some originate when large amounts of water are released from subglacial streams at the termination of a surge (Kamb et al., 1985). Others involve the release of water from lakes dammed when a surging glacier blocks a side valley (Truffer et al., 2021). Floods from glacier-dammed lakes can occur in several ways (Allen et al., 2022). One involves the formation and enlargement of tunnels under or through the glacier. Repeated GLOFs can occur as these tunnels enlarge, collapse, and reform (Kienholz et al., 2020; Haeberli and Drenkhan, 2022). Another GLOF mechanism involves the sudden collapse of an ice dam (Haeberli, 1983; Jacquemart and Cicoira, 2022). These ice-dam collapses produce some of the largest and most destructive GLOFs (Bhambri et al., 2019; Bazai et al., 2022). GLOFs triggered by the collapses of ice dams can cause sudden, extreme flows downstream, which, depending on the volume of the glacier-dammed lake (Walder and Costa, 1996), can transport large icebergs along with large amounts of rock debris (Carrivick and Tweed, 2019; Huber et al., 2020; Cook et al., 2021). A key contributing factor to GLOFs triggered by ice-dam collapses is the shattered nature of the glacier's terminus after a surge. Once the surge ends, the crevasse-shattered ice near the terminus is not being replaced by ice flowing from above, which makes the terminus particularly susceptible to ice-dam collapses (Walder and Costa, 1996; Truffer et al., 2021).

3. Study area

The BRG (Fig. 1 and 2) is a 40-km long, surge-type glacier located in the eastern Alaska Range (Heinrichs et al., 1996). It extends from 3650 m asl down to 700 m and has a median altitude of 1850 m (Kienholz et al., 2017). The lower reaches of the BRG lie in a bedrock trench excavated by glacial erosion along the strike-slip McKinley Strand of the Denali Fault (Stout et al., 1973; Péwé and Reger, 1983). The last major earthquake along this fault segment was a magnitude 7.9 earthquake in 2002 (Koehler and Carver, 2018). This earthquake triggered landslides that covered 12 km^2 of the lower glacier and caused localized changes in the glacier's topography and flow velocity (Shugar et al., 2012); however, the supraglacial debris added by these landslides caused only a minor reduction in the glacier's overall ablation rate (Kienholz et al., 2017).

The BRG last surged in 1936-7 (Hance, 1937; Moffit, 1942; Geist and Péwé, 1957). Its reservoir zone thickened between 1950 and 1995 (Shugar et al., 2010), but the overall glacier showed no net gain of mass between 1980 and 2010 (Kienholz et al., 2017). Widespread glacier melt has been underway throughout the Alaska Range over the last several decades (Larsen et al., 2015), and modelling suggests the BRG will continue to down-waste and retreat into the next century, which implies it is incapable of surging in the near future (Heinrichs et al., 1996; Kienholz et al., 2017)

Bedrock in the study area is pelitic greenschist and amphibolite (Nokleberg et al., 1990). An outcrop of greenish, fine-grained amphibolite occurs where Falls Creek exits the former Rapids Lake marginal channel over a small cascade and then veers westward to join the Delta

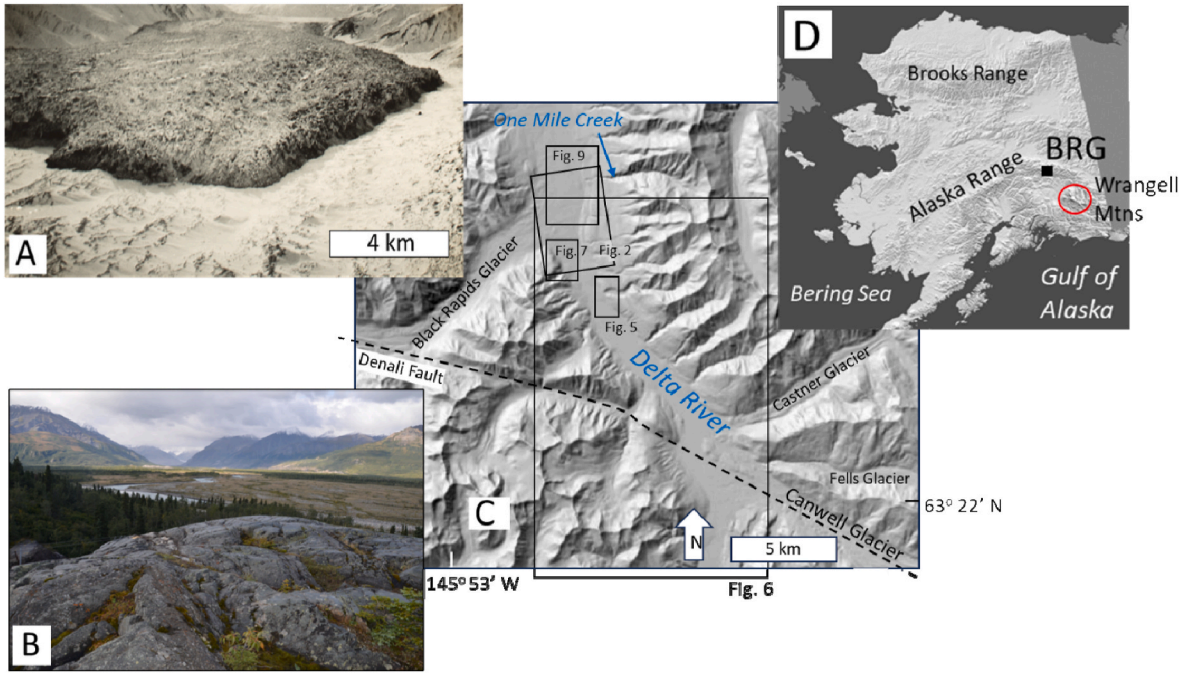

Fig. 1. A. An oblique, aerial photograph looking westward up the Black Rapids valley showing the surging BRG on March 11, 1937 (W. B. Drawbaugh, University of Alaska Archives). The face of the advancing terminus was estimated to be 60–150 m high, and the glacier advanced ~5 km during the late autumn and early winter of 1936-7 (Hance, 1937). **B.** View westward up the Black Rapids valley in 2022 from the Amphibolite Knob at Camp Terry (Fig. 2). The down-wasting terminus of the glacier is barely visible in the distance. **C.** Location of the study area in the eastern Alaska Range. The digital elevation map of Alaska is from Riehle et al. (1997). **D.** Location of the BRG and the Wrangell Mountains.

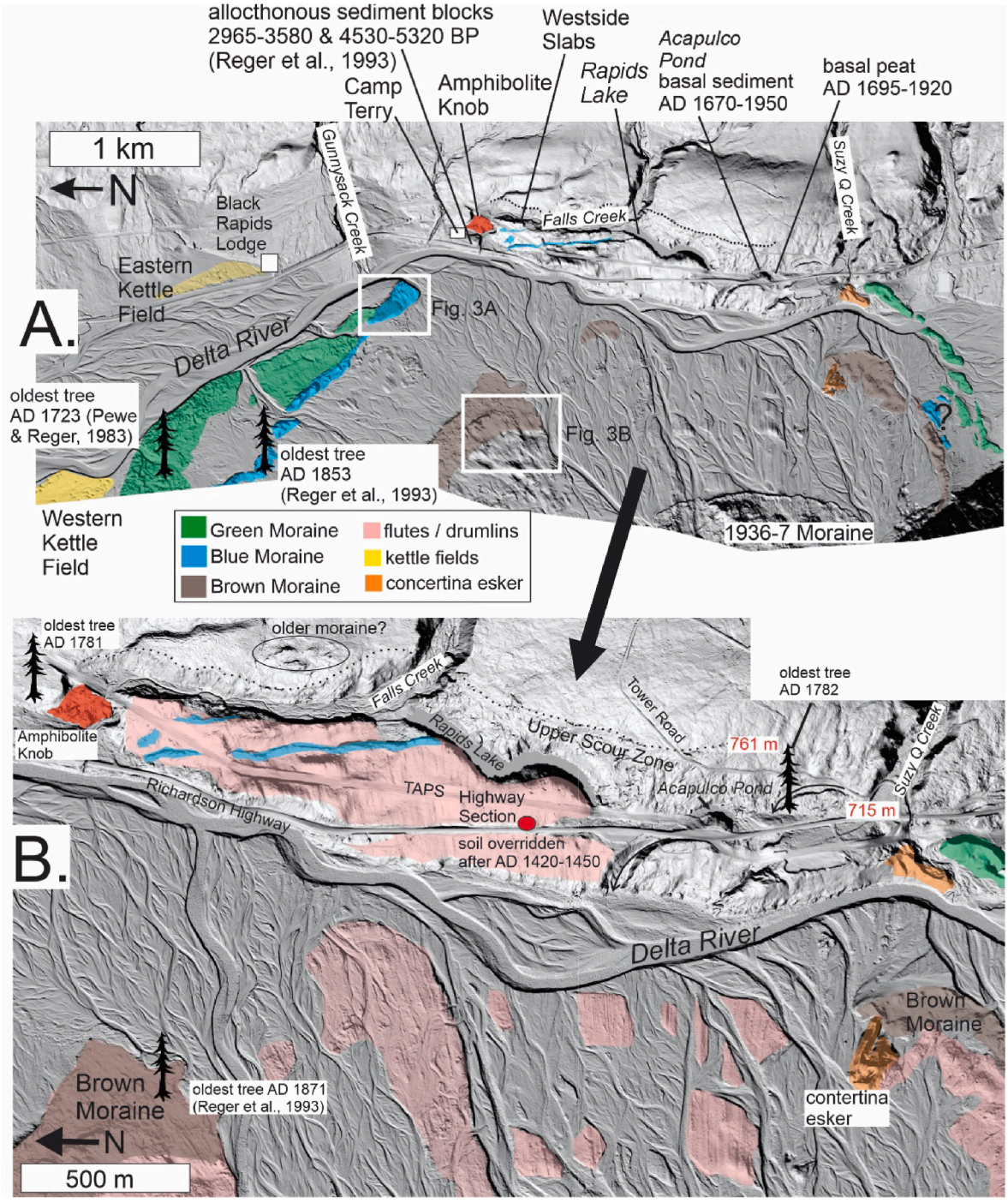

Fig. 2. Landforms on the BRG foreland along with ^{14}C and dendrochronological dates constraining their ages. Uncited tree ages are from this study. The Highway Section (red dot) is described in Section 6.2. **A.** Overview of the glacier foreland. **B.** Enlarged view of the central foreland area showing the extent of the streamlined till plain (pink shading). "TAPS" is the Trans-Alaska Pipeline System.

River (Figs. 1B and 2B). The regional climate is continental subarctic (Köppen Dfc) (Shulski and Wendler, 2007). At the nearest weather station, Delta Junction 70 km north and 350 m lower that the BRG foreland, July has the warmest average temperature (11 °C), January has the coldest (−22° C). Peak precipitation occurs in autumn (August–October) (Bieniek et al., 2022).

Treeline is located at 850–900 m asl. White spruce (*Picea glauca*) is the dominant conifer species. The oldest spruce trees occur as scattered individuals emerging from an understory of alders (*Alnus siberica*) on the older portions of alluvial fans. Permafrost is discontinuous in the area, and tree growth is limited by cool soil temperatures, as evidenced by the persistence of frozen soil into early August beneath the root masses of old trees (Section 6.2.1). In response to the cold soils and the rapid deposition of loess, white spruce trees send out adventitious roots near the ground surface as their older, deeper roots die. Observations of primary succession on the Black Rapids foreland suggest that the ecesis

(the period of tree establishment and growth to ~ 50 cm height) of white spruce requires approximately 20 years (Péwé and Reger, 1983; Reger et al., 1993).

4. Previous studies

By Alaskan standards, the BRG has a long history of glacial geological studies. Mendenhall (1900) visited the area in 1898 and noted a fresh-looking moraine (our Brown Moraine). The 1936-7 surge brought the glacier to the attention of numerous observers (Giddings, 1988). Hance (1937) visited the surging BRG in the winter of 1937 by airplane, photographed its advancing front, and described in detail the shattered glacier terminus. Photographs taken at that time (Fig. 1A) show the terminus ploughing across a treeless glacial foreland. Based on climate records from Fairbanks 200 km to the northwest, Hance (1937) suggested that unusually heavy snowfalls during the preceding decade caused the 1936-7 surge. Bradford Washburn dispatched two representatives of the Harvard Institute of Geographical Exploration to inspect the glacier in the summer of 1937. Otto Geist of the University of Alaska made multiple visits to the Black Rapids area (Geist and Péwé, 1957). Moffit (1954) visited in September of 1937 to view the surge, which had ceased movement by that time. He noted the presence of two older moraines lying outside the limit reached in 1937 and speculated that they were left by prehistoric surges. Moffit (1942) cited the opinion of Tarr and Martin (1914) that glacial surges consisted of cycles of rapid advance followed by lags whose durations depended on the replenishment of ice in a reservoir zone in the upper glacier. Péwé (1951) noted the presence of two older moraines outside of the 1936-7 surge limit, and cored and dated spruce trees in the area. Péwé and Reger (1983) and Reger and Péwé (1991) used dendrochronology and lichenometry to date moraines of the Black Rapids, Canwell, and Castner Glaciers, which they inferred had fluctuated coevally. Péwé and Reger (1983) identified Rapids Lake (their "Hidden Lake") as a marginal channel carrying the Delta River when the BRG dammed the valley. Post and Mayo (1971) mapped two sets of former shorelines in the Delta River valley upstream of the BRG and attributed them to glacier dams formed during prehistoric surges (Moffit, 1954).

Reger et al. (1993) synthesized earlier investigations of the glacial history of the Black Rapids area and reported new radiocarbon dates, along with a revised lichenometric chronology. They also identified two, pre-1936-7 moraines on the eastern side of the Delta River. Reger et al. (1993) attempted to correlate the stratigraphy of the truncated alluvial fans bordering the Black Rapids foreland with episodes of erosion/incision occurring during the glacier's advances. They obtained ^{14}C dates between 3400 and 5300 cal yr BP on turf layers that Péwé and Reger (1983) had discovered in allochthonous blocks of outwash material stranded on the eastern side of the Delta River near the mouth of Falls Creek. They suggested these blocks were transported by the surge that deposited their "Oldest Holocene Moraine" (our Green Moraine) (Fig. 2). Based on the available chronological information, Reger et al. (1993) suggested the Green and Blue Moraines were deposited by surges between 1710 and 3360 cal yr BP, and that their "Youngest Holocene Moraine" (our Brown Moraine) (Fig. 2) was deposited before ca. AD 1420. They acknowledged this chronology was incomplete and that other advances probably occurred.

The chronologies of the Castner and Canwell Glaciers (Fig. 1) are of interest because of the proximity of these apparently non-surging glaciers to the BRG. Calkin (1988) speculated that the Canwell Glacier was a surge-type glacier; however, there are no historical records of it surging. Unlike the BRG and other known surge-type glaciers in the Alaska Range (Post, 1972; Herreid and Truffer, 2016), the Canwell Glacier lacks signs of flow instability in the form of distorted or looped medial moraines. A date of 225 ± 90 ^{14}C yr (GX-15535) on organic material embedded in the youngest terminal moraine of the Canwell Glacier indicates it was constructed after 425 cal yr BP (Reger and Péwé, 1991). When calibrated in CALIB 8.2, the most probable age range of this ^{14}C date at 1-sigma is 140–225 cal yr BP. The oldest tree growing on the younger of the Canwell Glacier's two moraines was 102 years old in AD 1951 (Péwé and Reger, 1983). After subtracting 20 years to account for ecesis, this tree age provides an upper-limiting date of ca. 1829 for moraine construction.

Based on its length and topography, Wilbur (1988) speculated that the Castner was a surge-type glacier; however, no surges have been observed, nor is there any evidence from looped medial moraines that the Castner Glacier surges. Howley (2008) dated the youngest moraine of the Castner Glacier to between AD 1834 and 1842 on the basis of cosmogenic and lichenometric dating, respectively. Howley (2008) also dated the penultimate moraine of the Castner Glacier to AD 1626 ± 32 and AD 1692 on the basis of cosmogenic and lichenometric dating, respectively.

5. Methods

5.1. Geomorphic mapping, delineation of paleo-lakes, and estimates of flood discharges

We used LiDAR imagery obtained by the Infrastructure Corridor Project of the Alaska Department of Transportation in 2011 and made available through the Alaska Division of Geological & Geophysical Surveys (https://elevation.alaska.gov/#63.39583:-145.50842:10). We used hill-shading with bi-linear resampling and adjusted the Z Factor, brightness contrast and light perspective to accentuate geomorphic features. We estimated the volume and extent of lakes formed when the BRG dammed the Delta River by first tracing their shorelines visible on the IFSAR digital surface model (Carswell, 2013) along the eastern side of the Delta River valley. To estimate lake volumes, we took the mean elevation of each shoreline and used the 'Raster Surface Volume' processing tool applied to the Arctic DEM digital surface model in QGIS software. Estimates of peak discharge for the glacial lake outburst floods during tunnel-flow and dam-collapse scenarios were calculated using the equations of Clague and Mathews (1973), Costa (1988), Walder and Costa (1996), and Ng and Björnsson (2003).

5.2. Stratigraphy and radiocarbon dating

Stratigraphic archives were investigated and radiocarbon-dated to constrain the BRG's history. This includes the collection and analysis of lake sediment records from Rapids Lake and Acapulco Pond (Fig. 2A). Both lakes were cored through the ice using a modified Livingston corer (Wright et al., 1984). Stratigraphic sections were exposed using hand tools. ^{14}C dates on charcoal, wood, and plant macrofossils were calibrated using Calib 8.2 (http://calib.org/calib/) and the IntCal20 Calibration Curve (Reimer, 2020).

5.3. Lichenometry

Lichenometry (Winchester, 2023) is useful for establishing the relative ages of geomorphic surfaces where saxicolous lichens grow (Rosenwinkel et al., 2015). The use of lichenometry as a dating method has been repeatedly criticized (e.g., McCarthy, 2021; Osborn et al., 2015), yet it continues to find numerous applications (e.g., Benedict, 2009; Bradwell, 2009; Winchester, 2023). One of the method's main challenges involves constructing a calibration curve that relates lichen size to known surface-exposure age (McCarthy, 2021; Solomina and Calkin, 2003; Wiles et al., 2010). Ideally, calibration curves are site-specific because lichen growth rates vary in response to altitude, moisture, growing degree days, wind exposure, rock type, competition between lichens, and shading by vascular plants (Trenbirth and Matthews, 2010). Changes in microclimatic and ecological conditions over time can make the relationship between lichen size and surface age nonstationary (Benedict, 1990; Loso and Doak, 2006; Roof and Werner, 2011; Trenbirth and Matthews, 2010). As a result, calibration curves

become increasingly problematic on surfaces older than several centuries (Winchester, 2023). In their review of lichenometry in Alaska, Wiles et al. (2010) follow Ellis and Calkin (1984) and Solomina and Calkin (2003) in suggesting that lichenometric age estimates have errors of roughly ±20%.

In this study, we measured the longest diameters of circular thalli of *Rhizocarpon geographicum sensu lato* (Benedict, 2008) using digital calipers. These measurements have an accuracy of ±1 mm (O'Neal et al., 2013). We assume that lichen establishment occurred within several years after surface exposure and stabilization (Winchester and Sjöberg, 2003). Between 50 and 240 individual *Rhizocarpon* thalli were measured at each site. A site was considered an area >5000 m^3 where >50 large boulders are exposed without a tree overstory. The diameters of the largest five lichen from each geomorphic surface were then averaged. Lichens that were >20% larger than the mean of the next five, largest lichens were excluded from the analysis. To establish a lichen age-growth calibration curve, we measured lichens growing on six geomorphic surfaces of known ages within the study area and then modeled the resulting age-growth relationship.

5.4. Dendrochronology

White spruce trees were used for dendrochronology. Because heart rot is ubiquitous in trees older than 100 years, it was necessary to fell trees and sample entire cross sections from their lower trunks. Working with cross-sections enabled us to work around rotten areas and obtain complete records of annual rings. The tree ages reported here are the pith ages of measured cross sections taken 1–2 m above the ground. Cross-sections were sanded with progressively finer sandpaper up to 800 grit. Ring widths were digitally measured to 0.001 mm using high-resolution scans uploaded to the computer program CooRecorder 8.1. Ring-width series were visually and statistically cross-dated using standard dendrochronological techniques (Holmes, 1983; Stokes, 1996). Chronologies of ring width indices (RWIs) were compiled by first detrending individual series with a negative exponential curve and then obtaining the bi-weight robust mean of individual ring-width indices using the dplr package in R studio (Bunn, 2008).

Dendrochronology aids the interpretation of the glacier and flood history of the BRG in three ways: 1) The pith ages of living trees provide minimum-limiting dates on when a particular geomorphic surface was established. 2) The outermost annual rings of cross-dated trees buried by delta deposits provide maximum-limiting dates on proglacial lake formation. These buried trees were cross-dated with previously measured, calendar-dated chronologies using correlation analysis and then visually checked for shared marker years using skeleton plots generated by the CDendro software and the dplr package in Rstudio (Bunn, 2008). 3) Changes in growth rates provide a proxy for shifts in periglacial microclimate (Gaglioti et al., 2022) caused by changing proximity to the BRG, to proglacial lakes, as well as to icebergs stranded after glacial lake outburst floods (GLOFs).

We looked for shifts in periglacial microclimate by comparing the ring-width indices (RWIs) of trees growing near the glacier, proglacial lakes, and GLOF deposits with trees growing further away. These comparisons take the form of ratios between RWIs. We compared two different sets of tree-ring chronologies over different time intervals. For the AD 1600–1800 interval, trees growing at the Lower and Upper fan sites on the alluvial fans of One Mile Creek (Fig. 1) provide the tree-ring record nearest the Black Rapids foreland. The RWIs of these trees are compared with white spruce growing in the Wrangell Mountains 250 km to the southwest (Davi et al., 2011), as well as with trees growing in Central Alaska (Interior Alaska), 100–400 km to the northwest (D'Arrigo et al., 2006). Although they are located at a distance of 1.5 km from the nearest moraine of the BRG, trees at the Lower and Upper fan sites were exposed to a GLOF that stranded large numbers of icebergs nearby (Section 6.2.1). Between AD 1800 and 2000, we used the RWIs of trees growing at the Upper and Lower fan sites on the alluvial fan of One Mile Creek as the control and compared them with trees growing closer to the glacier near Acapulco Pond (Fig. 2B). Ca. AD 1800, spruce trees colonized the area around Acapulco Pond, which meant that at times they were <500 m from the terminus of the BRG and its proglacial lake. At this distance, glaciogenic effects on microclimate and on tree growth can be pronounced (Gaglioti et al., 2022, 2024).

5.5. Estimating lags in glacier responses to climate changes

We estimated the lags in glacier responses to changing climate using the empirical relationship developed by Zekollari et al. (2020) for the European Alps:

$$T = 121–1.24*\alpha_{80\%} - 0.028*\Delta_Z$$

where T (years) is glacier response time, $\alpha_{80\%}$ (%) is surface slope along the flowline of the lowest 80% of the glacier, and Δ_Z (m) is the glacier's overall elevational range.

6. Results

6.1. Geomorphic mapping

6.1.1. Glacial deposits

Four terminal moraines and an assortment of the glacial features frequently associated with surge-type glaciers are present in the foreland of the BRG (Fig. 2A). We designated the moraines with colors rather than numbers or letters in order to avoid assumptions about their ages. The Green Moraine corresponds to Reger et al.'s (1993) "Oldest Holocene Advance", the Blue Moraine corresponds to their "Intermediate Holocene Advance", and the Brown Moraine corresponds to their "Youngest Holocene Advance".

Deposits characteristic of surge-type glaciers (Sharp, 1988; Evans and Rea, 1999; Schomaker et al., 2014; Ingólfsson et al., 2016) occur in association with all four of these moraine systems. East of the Delta River, an extensive fluted till plain (Fig. 2B; 3) is indicative of water-saturated, subglacial sediment that flowed into low-pressure zones in the lee of either bedrock obstructions and/or moving boulders (Hart, 1995; Kjær et al., 2016). Fragments of this flute and drumlin terrain also occur west of the river in places where it has escaped erosion by streams. Crevasse-squeeze ridges (Sharp, 1985) occur in patches within former moraine margins (Fig. 3B). Considered diagnostic of surge-type glacier deposits (Farnsworth et al., 2016; Aradóttir et al., 2019), crevasse-squeeze ridges form when saturated sediment is pushed upwards into bottom-up crevasses developed within a surging ice mass (Rea and Evans, 2011; Ben-Yehoshua et al., 2023).

Distinctive features of the moraines in the Black Rapids foreland attest to their origin during surges. Their distal edges are formed by narrow (<10 m) "rim walls", behind which lie a confusion of multiple, subsidiary moraine crests and hummocky supraglacial tillthat has been fluted by overriding ice (Fig. 2a). Where exposed along the Delta River opposite Black Rapids Lodge (Fig. 2A), the internal structure of the Green Moraine is consistent with that of a thrust-and-stacked moraine (Benediktsson et al., 2015; Ingólfsson et al., 2016) that overlies a wedge of sediment probably originating from an alluvial fan of Gunnysack Creek (Fig. 2A). The multiple, subsidiary moraine crests present within the Green, Blue, Brown, and 1936-7 moraines represent submarginal moraines (Benediktsson et al., 2009) formed when the glacier overrode unconsolidated and saturated sediment near the end of its surge. The Green Advance, or perhaps an earlier one, carried intact blocks of outwash sediment across the river and deposited them near Camp Terry (Fig. 2A). Reger et al. (1993) believed these blocks were transported in a frozen state, which is consistent with a surge occurring in winter.

Other geomorphic features in the Black Rapids foreland typical of surging glaciers include hummocky moraines and concertina (zig-zag) eskers (Ingólfsson et al., 2016) (Fig. 4A and B). The latter are uncommon

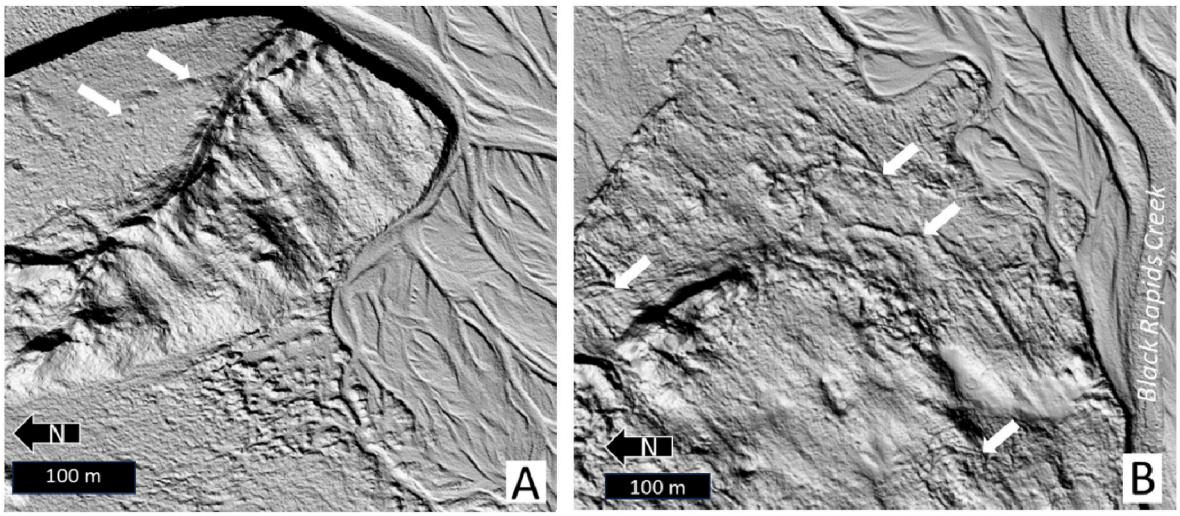

Fig. 3. Deposits in the BRG foreland characteristic of surge-type glaciers. **A.** The distal end of the northern loop of the Blue Moraine west of the Delta River. Arrows point to examples of pitted outwash. A narrow "rim wall" forms the moraine's distal edge while the bulk of the moraine consists of a wedge of outwash-derived sediment that was fluted and drumlinized by overriding ice. An area of hummocky moraine is visible in the lower center of the image. **B.** A portion of the Brown Moraine showing numerous flutes and drumlins. Arrows indicate crevasse-squeeze ridges.

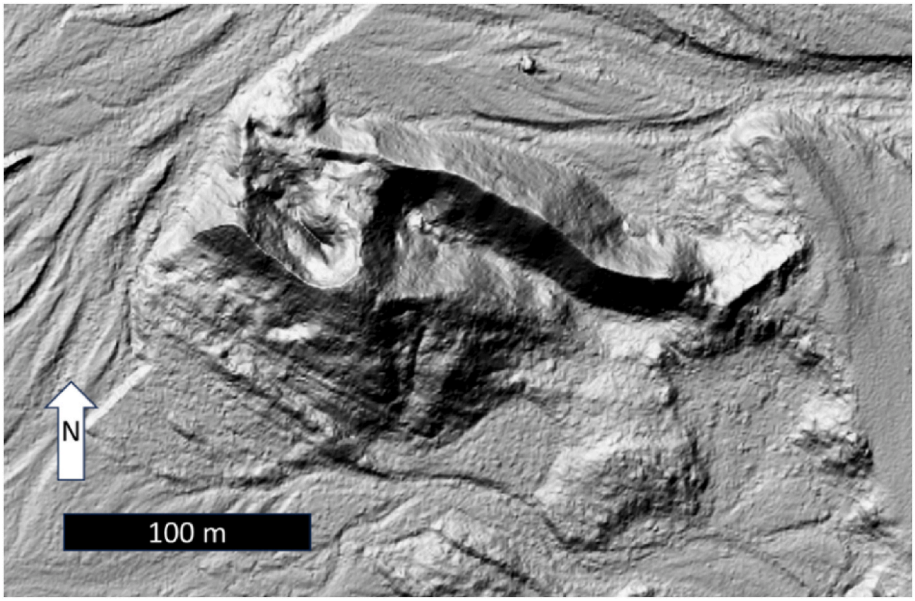

Fig. 4. A concertina esker on the proximal side of the southern loop of the Brown Moraine (Fig. 2). This feature is 5–10 m high. Another, possible concertina esker occurs near the junction of Suzy Q Creek and the Delta River (Fig. 2A).

but distinctive features left by surging glaciers. They form during the closing phases of a surge when supraglacial or englacial meltwater streams deposit sediment within chaotically interconnected crevasse systems (Evans and Rea, 2016). Pitted outwash is another feature common on the forelands of surge-type glaciers (Fig. 3a), and extensive areas of pitted outwash occur downstream of the Green Moraine (Section 6.1.5). The presence of pitted outwash, hummocky moraine, crevasse-squeeze ridges, concertina eskers, and fluted/drumlinized terrain are consistent with all four of the BRG's moraines having formed during surges.

6.1.2. *Marginal channels and glacier-dammed lakes*

A marginal channel carrying the Delta River flowed through Acapulco Pond, Rapids Lake, and lower Falls Creek when the BRG dammed the valley (Péwé and Reger, 1983). This channel emptied onto the Amphibolite Knob (Fig. 2A), which was eroded and polished by sediment-laden water. Rapids Lake is now dammed by a fan of sediment spilling over from the floodplain of Falls Creek. Echo sounding and sediment coring revealed that both Rapids Lake and Acapulco Pond are floored by large boulders. Water depths are only 1–3 m, and many of these boulders protrude from the water surface. The size of these boulders, their exotic lithologies, and their water-worn shapes, along with the dimensions of the paleo-channel are consistent with this channel system once carrying the entire flow of the Delta River. Other channel segments are incised into bedrock between Acapulco Pond and Tower Road (Fig. 2B). Lying at an elevation of ~715 m asl, this area was probably the outlet threshold of multiple lakes dammed in the upper Delta River valley by the BRG.

LiDAR imagery reveals a scour zone upslope of the Acapulco Pond-Rapids Lake-Falls Creek marginal channel (Fig. 2A and B). The colluvium in this Upper Scour Zone has been largely removed. We interpret this scour zone as the result of erosion by the diverted Delta River when

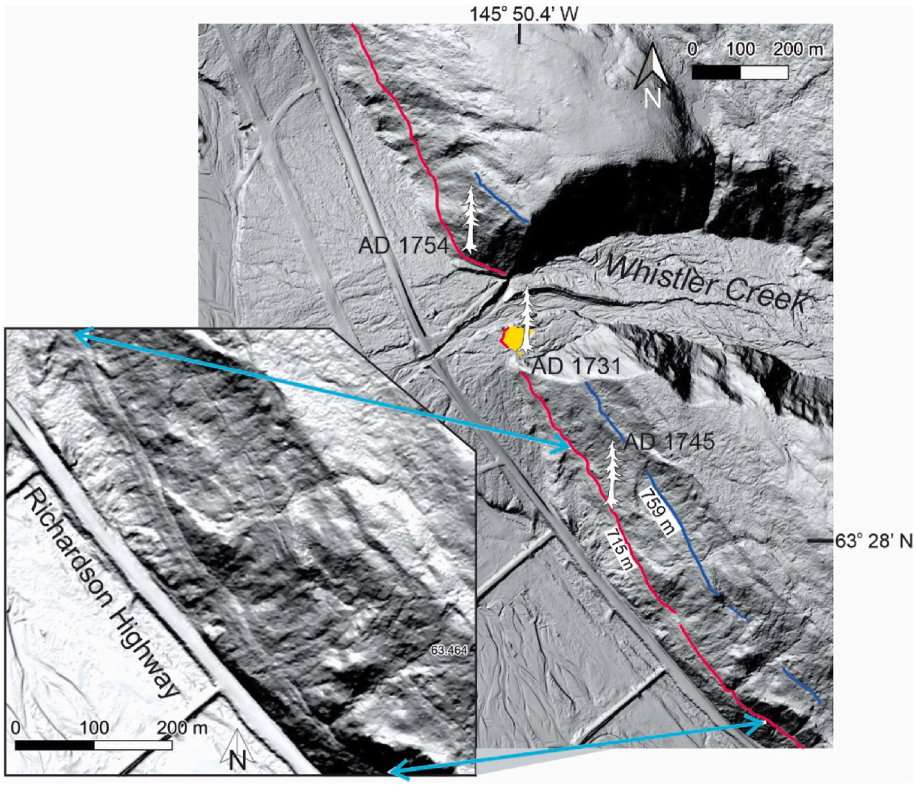

Fig. 5. Paleo-shorelines of Upper (blue line) and Lower (red line) Glacial Lake Whistler on the eastern side of the Delta River valley near the mouth of Whistler Creek. The yellow polygon is the surface of the paleo-delta built into Lower Glacial Lake Whistler. The uncorrected pith ages of white spruce are shown beside the tree images. The inset panel shows the Upper and Lower shorelines at higher magnification. Note the multiple subsidiary berms of both shorelines and the poorer preservation of the Upper Shoreline.

Table 1
Altitudes estimated from the IFSAR digital surface model of geomorphic features related to glacier-dammed lakes in the Delta River valley. The shoreline of Upper Glacial Lake Whistler is confluent with the top of the Upper Scour Zone above Rapids Lake and Acapulco Pond. The shoreline of Lower Glacial Lake Whistler is confluent with the Westside Shoreline and with the surface of the Whistler Creek delta.

	Lower Shoreline	Upper Shoreline	Acapulco Pond	Rapids Lake	Base of Upper Scour Zone	Top of Upper Scour Zone	Castner Glacier area Upper Shoreline	Westside Shoreline
Count	15	15	15	15	15	15	15	15
Mean (m)	**715**	**759**	**707**	**704**	**743**	**761**	**759**	**715**
SD (m)	0.39	0.30	0.24	0.00	0.99	3.04	0.55	0.86

Upper Lake Whistler (Fig. 5) was dammed by the glacier. As the ice dam down-wasted, the diverted river probably tracked it downslope. As measured using the LiDAR imagery, the upper edge of the Upper Scour Zone is confluent with the highest shoreline of Upper Glacial Lake Whistler (Fig. 5) and lies approximately 54 m above the surface of Acapulco Pond (Table 1).

Two sets of shorelines were left by lakes dammed in the upper Delta River valley by the BRG. The highest shoreline (Upper Glacial Lake Whistler) is preserved intermittently at 759 m asl along the alder-choked, eastern side of the valley upstream of the Black Rapids foreland (Figs. 6). Dense vegetation makes this shoreline difficult to trace on the ground. Approximately 44 m downslope, the shoreline of Lower Glacial Lake Whistler is better developed and preserved. Three to four, minor shorelines occur below the main one within an altitudinal band of 10 m (Figs. 5 and 6). The shoreline of the Lower Lake can be traced southwards along eastern valley wall to 1 km north of TAPS Pump Station 10. The shoreline of the Upper Lake extends 3 km further south where it intersects outwash deposits of the Castner Glacier (Fig. 6). Regrettably, there is no clear cross-cutting relationship between the shoreline of Upper Glacial Whistler and the moraines of the Castner Glacier.

The shoreline of Lower Glacial Lake Whistler can also be detected along the western side of the Delta River valley where it cross-cuts the outermost moraine, which we assume is the Green Moraine due to its position (Figs. 7). Dense vegetation prevented sampling lichens on this moraine. Even if lichens could have been measured, because this moraine was submerged by Lower Glacial Lake Whistler, it could not be distinguished using lichenometry from the Blue Moraine that dammed this lake.

6.1.3. *Estimates of GLOF discharges from Glacial Lake Whistler*

The relationship between lake volume and discharge during jökulhlaups (GLOFs) has been extensively measured and modeled (Clague and Mathews, 1973; Bjornsson, 1992; Walder and Costa, 1996; Westoby et al., 2014; Worni et al., 2014; and numerous other case studies). Keeping in mind the caution of Walder and O'Connor (1997) that such estimates are highly dependent on the rate of water release, Table 2 lists some possible peak discharges from Upper and Lower Glacial Lake Whistler. Ice dam failures are the most likely trigger for GLOFs from lakes dammed by the surges of the BRG because of the shattered nature of the post-surge terminus (Truffer et al., 2021). Based on these estimates, discharge during the catastrophic drainage of the

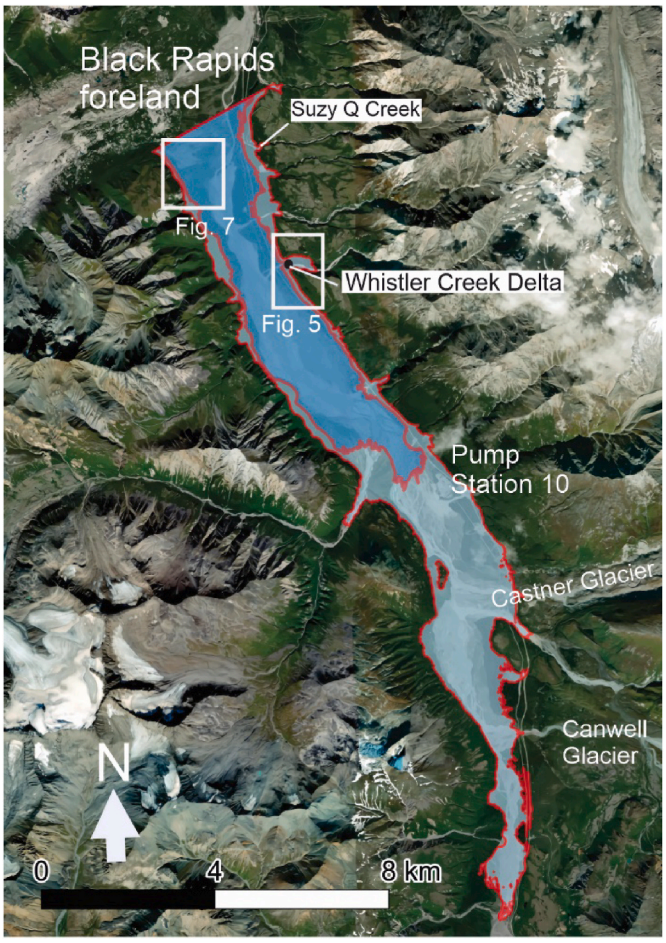

Fig. 6. The approximate extents of Upper (lighter blue) and Lower (darker blue) Glacial Lake Whistler dammed by surge advances of the BRG.

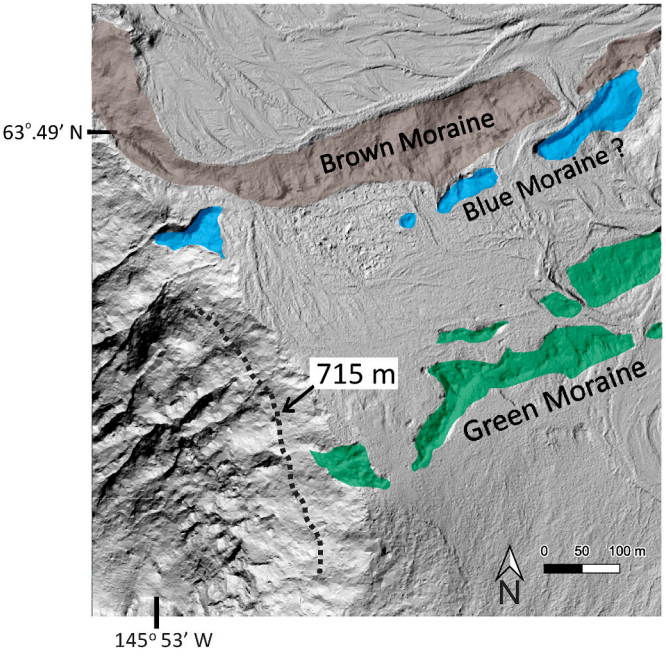

Fig. 7. Traces of the shoreline of Lower Glacial Whistler (dashed black line) occur at 715 m asl on the western side of the valley adjacent to the southernmost moraines of the BRG.

upper lake might have reached 18,000 m^3s^{-1}, and discharge from the lower lake might have reached 10,000 m^3s^{-1} (Table 2). For comparison, the mean discharge of the Yukon River at Stevens Village at peak annual flow in June is 10,500 $m^3\ s^{-1}$ and 2260 $m^3\ s^{-1}$ for the Tanana River at Nenana, respectively (United States Geological Survey National Water Information United States Geological Survey National Water Information System, 2024).

6.1.4. *Whistler Creek Delta*

Stream erosion exposed a Gilbert-type delta along lower Whistler Creek in the autumn of 2020 at N 63° 28.211′, W145° 50.453′ (Fig. 8). Today, Whistler Creek is a braided stream with a bedload of boulders. The delta's surface lies at the elevation of the shoreline of Lower Glacial Lake Whistler (Fig. 5). Unfortunately, this exposure was re-buried in 2022 by road work that channelized Whistler Creek. An alder branch from the uppermost foreset beds of the delta yielded a ^{14}C date of AD 1530–1790, which has a probability of p = 0.68 of lying between AD 1635 and 1665 (Table 3). The bottomset beds of the delta buried a forest of mature spruce and cottonwood trees growing on a well-developed soil. Two of the spruce stumps were dated using ^{14}C and dendrochronology. Because the ^{14}C ages of these trees fall within the twilight zone of radiocarbon dating, they are only useful for confirming the ages established by dendrochronology (Fig. 8). Cross-dating with trees growing on the alluvial fan of One Mile Creek (Section 6.4) indicates that Stump B grew between AD 1552 and 1665 and Stump C between AD 1563 and 1677. Based on these tree-ring ages, the rising waters of Lower Glacial Lake Whistler flooded the site ca. AD 1677. After subtracting twenty years to account for ecesis, the pith age of the oldest white spruce now growing on the Whistler Creek Delta indicates that its topset beds became subaerial again prior to AD 1711 (Fig. 5). Concerted search failed to discover a delta higher in the Whistler Creek valley corresponding to Upper Glacial Lake Whistler.

6.1.5. *Deposits of glacial lake outburst floods (GLOFs)*

Pitted outwash deposits in the form of kettle fields (Fig. 9) result from the melting of blocks of glacial ice partially buried by outwash. Pitted outwash is common in the forelands of surge-type glaciers (Ingólfsson et al., 2016) because floods frequently occur as the surge concludes, and blocks of ice are easily quarried from the surge-shattered terminus of the glacier. A special case of pitted outwash results when GLOFs carry blocks of ice far from the collapsing ice dam where they originate.

Three kettle fields formed by one or more GLOFs occur immediately down-valley of the BRG (Fig. 9). A fourth kettle field that we did not investigate lies 2.5 km northwest of the Northern Kettle Field on the western side of the Delta River, outside the area covered by the 2011 LiDAR. The Eastern Kettle Field has been extensively modified by human activity, but the Northern and Western fields are better preserved. All these kettle fields are distant from recent glacial limits, which is consistent with their origin during GLOFs from lakes dammed by the BRG. All four of the kettle fields are located near the valley's margins, suggesting they are remnants of more extensive deposits that once covered the entire valley floor downstream of the BRG.

The geomorphology of the kettle fields is also indicative of their origin during GLOFs. In the Northern Field (Fig. 10), kettles have obstacle-lee deposits on their down-valley sides (Fig. 11). These obstacle-lee deposits consist of boulder gravel and stand 1–2 m higher than the upstream edge of the same kettle. Many obstacle-lee deposits in the Northern Kettle Field are elongate down-flow. Similar geomorphology, including kettles with obstacle-lee deposits, has been described from jökulhlaup (GLOF) deposits in the forelands of surge-type glaciers in Greenland and Iceland (Russell, 1993; Maizels, 1997; Olszewski and Weckwerth, 1999; Burke et al., 2010).

Based on the sizes of the ice blocks once buried in the Northern Kettle Field, we infer that they were transported in a large-volume flood, stranded as the flood peaked, and then partially buried by sediment as

Table 2
Possible flood discharges from the lakes dammed in the upper Delta River valley by the BRG. *Tunnel release* occurs when the lake finds egress through tunnels melted through the ice. *Dam failure* occurs when an ice dam collapses.

	Estimated flood discharge (m^3 s^{-1})					
	Lake volume (m^3 x 10^6)	Clague and Mathews (1973)	Walder and Costa (1996) *tunnel release*	Costa (1988) *tunnel release*	Björnsson (1992) *tunnel release*	Walder and Costa (1996) *dam failure*
Upper Lake	**1177**	8562	4893	10,435	1856	24,695
Lower Lake	**296**	3394	1966	4311	146	13,449

the flood waned. After subtracting the thickness of recently infilled sediment, the largest kettle in the Northern Kettle Field is 7.5 m deep. Given the relative densities of ice and water, at least 6.8 m of water would have been required to float a 7.5-m square block of ice. Most GLOFs are hyper-concentrated with sediment and can have densities up to 1800 kg m^{-2} (Costa, 1985, 1988; Du et al., 2023), which implies that a 7.5-m iceberg could have been transported by a flow half of its height. Given the present-day topography of the Delta River valley near the Northern Kettle Field, a 3.5-m deep flood would have spread approximately 1.5 km across the valley floor and would have eroded scarps into the toes of the alluvial fans along the eastern side of the valley (Fig. 9). At least some of the GLOFs issuing from the lakes dammed by surges of the BRG (Table 2) were probably large enough to cause floods of this magnitude.

6.2. Stratigraphic sections

6.2.1. Northern kettle field

Wood fragments near the base of a pit dug in the Upper Alluvial Fan (Figs. 12) provide a minimum-limiting ^{14}C date of AD 680–870 for the formation of this portion of the fan (Fig. 12). Another pit excavated at the base of the escarpment separating the Lower Fan from the Northern Kettle Field exposed a series of forest layers composed of compressed moss, spruce needles, and twigs underlain by weakly developed Bw

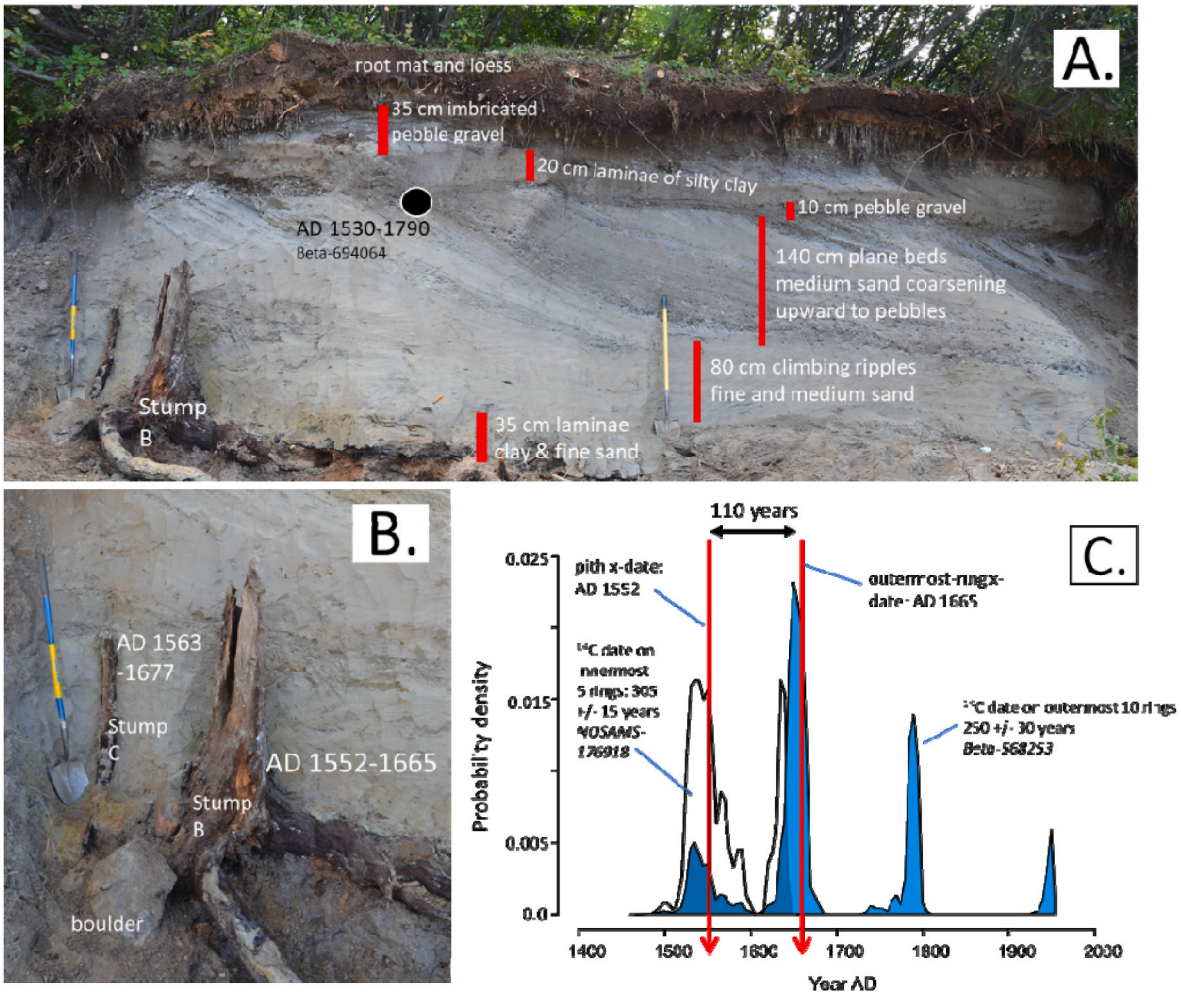

Fig. 8. A. The Whistler Creek Delta. This Gilbert-type delta was built into Lower Glacial Lake Whistler. The presence of a thin, upper set of bottomset and foreset beds suggests that brief, meter-scale fluctuations in lake level occurred near the end of the lake's existence. **B.** Two spruce trees were buried by delta construction. The age spans of their cross-dated annual rings are shown. **C.** Cross-dating the annual rings of Stump B from the Whistler Creek Delta with living trees in the area is consistent with the ^{14}C ages of its innermost and outermost rings. Ring-width indices from Stump B and C correlated with each other (R = 0.50) and with the overall Black Rapids tree-ring chronology (Section 6.4) (R = 0.47).

Table 3
Radiocarbon dates from the study area.

Laboratory Number	Sample name, location	^{14}C age (years BP)	δ^{13}C 0/00	1-σ calibrated age (2-σ calibrated age)	Most probable age range at 1-σ	Median age (year AD)
BETA-568253	outermost rings of large spruce Stump B, Whistler Delta	250 ± 30	−26.5	**AD 1530–1800** (AD 1520–1950)	AD 1640–1670 (p = 0.71)	1650
NOSAMS-176918	pith sample, Stump B, Whistler Delta	305 ± 15	−23.5	**AD 1520–1640** (AD 1520–1640)	AD 1520–1560 (p = 0.77)	1550
BETA-638004	bark of Stump C, Whistler Delta	150 ± 30	−25.4	**AD 1670–1940** (AD 1670–1950)	AD 1840–1880 (p = 0.26)	1810
Beta-694064	*Whistler30Aug2020B* detrital alder wood in uppermost Topset I unit of Whistler Delta	660 ± 30	−23.1	**AD 1530–1790** (AD 1520–1950)	AD 1635–1665 (p = 0.68)	1335
BETA-477317	9-1-17 B1 charcoal in upper alluvial fan, Camp Terry	2450 ± 30	−24.3	***2370-2700 BP*** *(2360–2700 BP)*	*2410-2500 BP* (p = 0.46)	*2520 BP*
BETA-543981	*2Sept2019KH#2* twig near base of kettle in Eastern Kettle Field	40 ± 30	−26.8	**AD 1690–1920** (BetaCal3.21)	–	–
BETA-543982	*9-9-17 C1* twig in Gunnysack Creek alluvial fan	4740 ± 30	−24.8	***5330-5580 BP*** *(5330–5580 BP)*	*5510 - 5580 BP (p=.068)*	*5510 BP*
BETA-543979	*7Sept2019A* twig near base of the Big Kettle, Northern Kettle Field	114 ± 0.4	−26.4	**AD 1695–1915** (AD 1690–1920)	AD 1880–1890 (p = 0.50)	AD 1845
BETA-543980	*20Oct2019C* twig at base of forest-floor loess, Upper Fan	1250 ± 30	−26.4	**AD 690–820** (AD 670–880)	AD 690–740 (p = 0.66)	AD 740
BETA-561547	*18June2020A* twig beneath tephra, underlying GLOF deposit	680 ± 30	−25.5	**AD 1280–1380** (AD 1280–1390)	AD 1280–1300 (p = 0.66)	AD 1335
BETA-561548	*18June2020B* twig above tephra, underlying GLOF deposit	660 ± 30	−25.0	**AD 1290–1390** (AD 1280–1390)	AD 1360–1390 (p = 0.55)	AD 1300
BETA-477319	*9-9-17A#1* Highway Section, twig in buried soil	480 ± 30	−25.3	**AD 1420–1450** (AD 1410–1450)	AD 1420–1445 (p = 1)	AD 1430
BETA-637999	*24Aug2019C* twig in peat below tephra, south end Acapulco Pond	110 ± 30	−25.2	**AD 1695–1920** (AD 1680–1940)	AD 1880–1920 (p = 0.34)	AD 1840
BETA-483494	*3M#1* twig in basal sediment of Acapulco Pond	160 ± 30	−25.8	**AD 1670–1950** (AD 1660–1950)	AD 1725–1780 (p = 0.43)	AD 1790

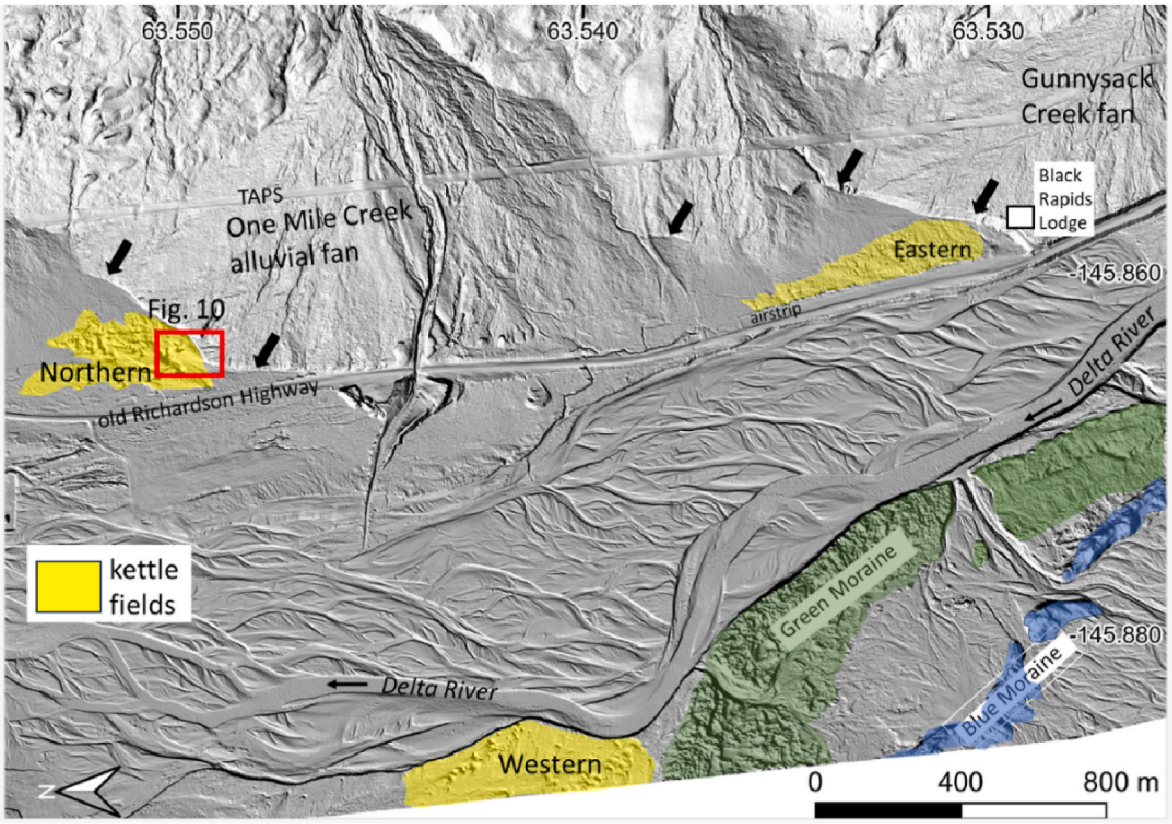

Fig. 9. The Delta River valley showing the locations of kettle fields (pitted outwash) relative to moraines of the BRG. Black arrows indicate scarps cut into distal alluvial fans, possibly by GLOFs.

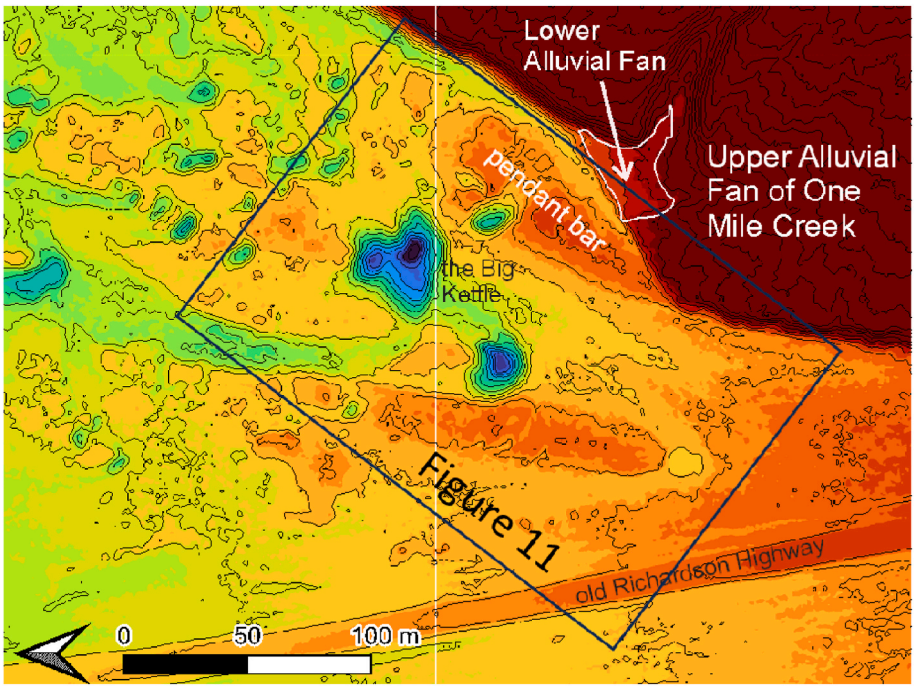

Fig. 10. Digital elevation model of the Northern Kettle Field based on LiDAR data. Contour interval ~1 m. Note the scarp truncating the alluvial fans. The pendant bar accreted in an eddy formed at the angle in the alluvial fan of One Mile Creek. Multiple icebergs were stranded within 100 m of trees growing at the Upper and Lower fan sites.

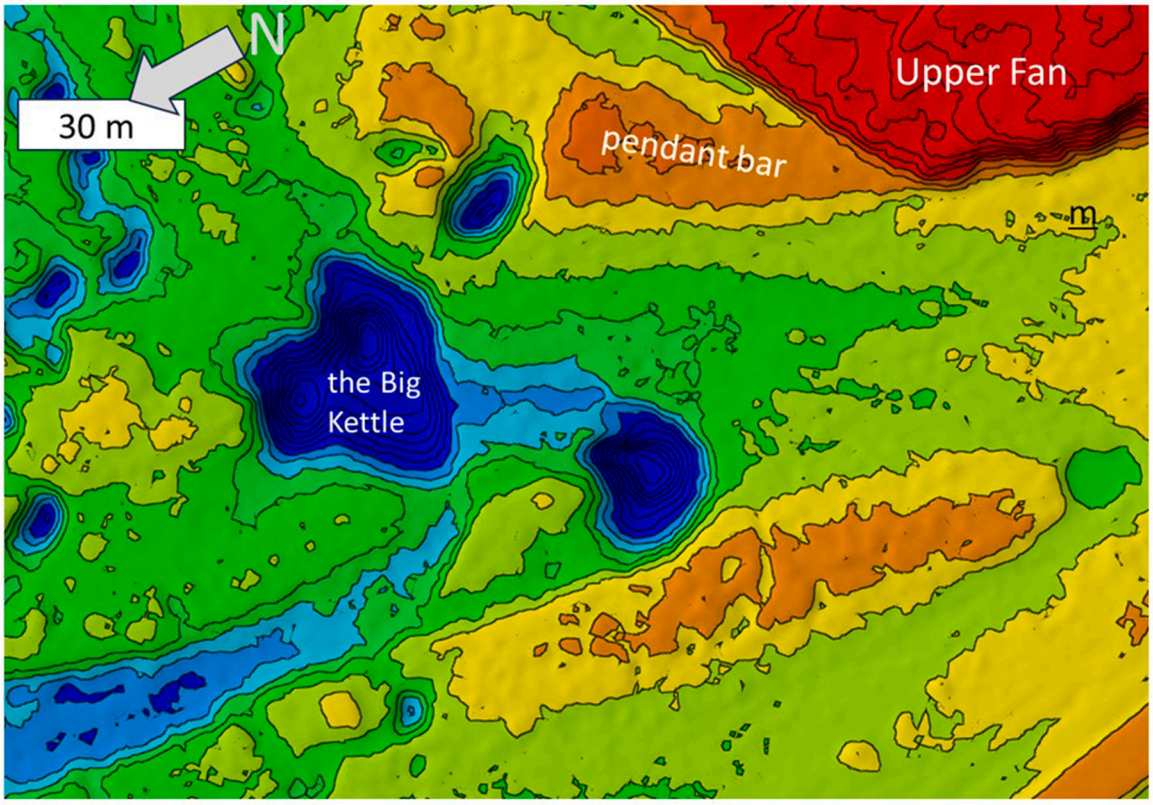

Fig. 11. Enlarged view of the topography of kettle holes and obstacle-lee deposits in the Northern Kettle Field. Contour interval ~1 m.

horizons. The forest layers were buried by layers of loess, which in turn were buried by 1.2 m of sand that was deposited in the lee of the pendant bar. Interbedded with the buried forest floors is a thin layer of grey tephra bracketed between ^{14}C ages of AD 1270 and 1390. An excavation in the bottom of the "Big Kettle" (Fig. 12) revealed 50 cm of silt and fine sand layers derived from recent flooding of One Mile Creek. This recent

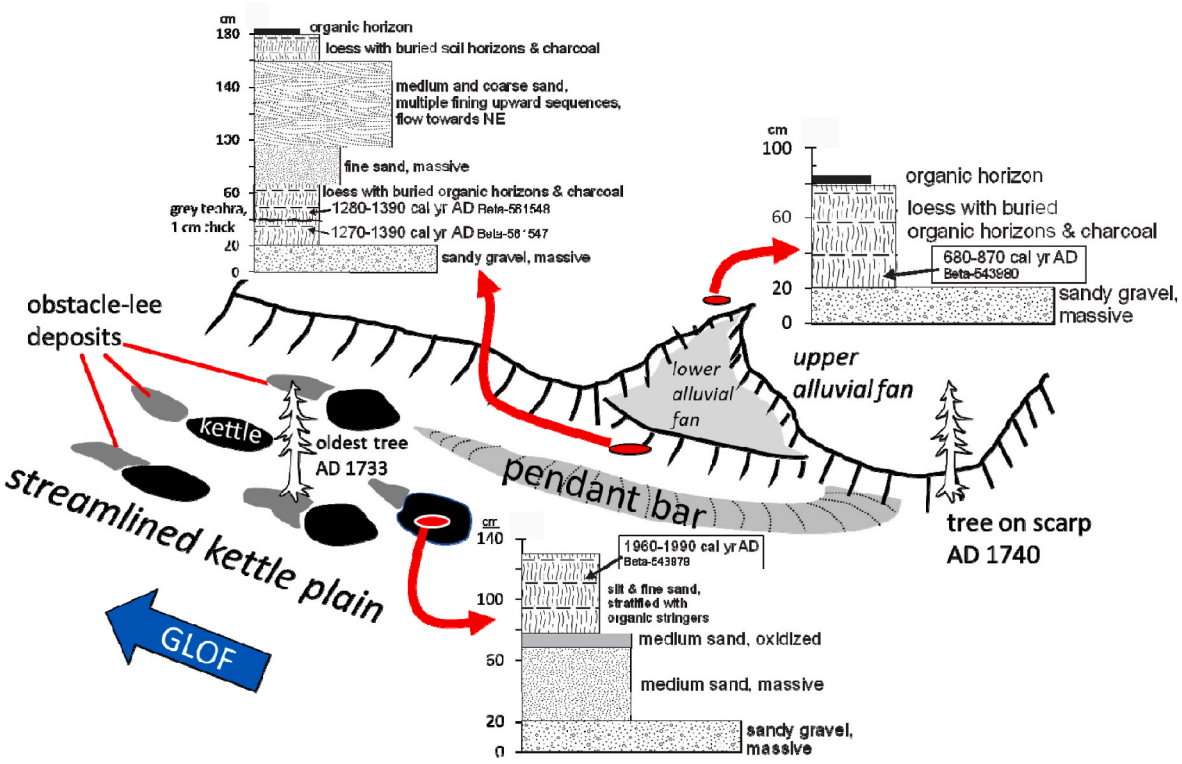

Fig. 12. Stratigraphy in the vicinity of the Northern Kettle Field. Red ovals indicate locations of soil pits.

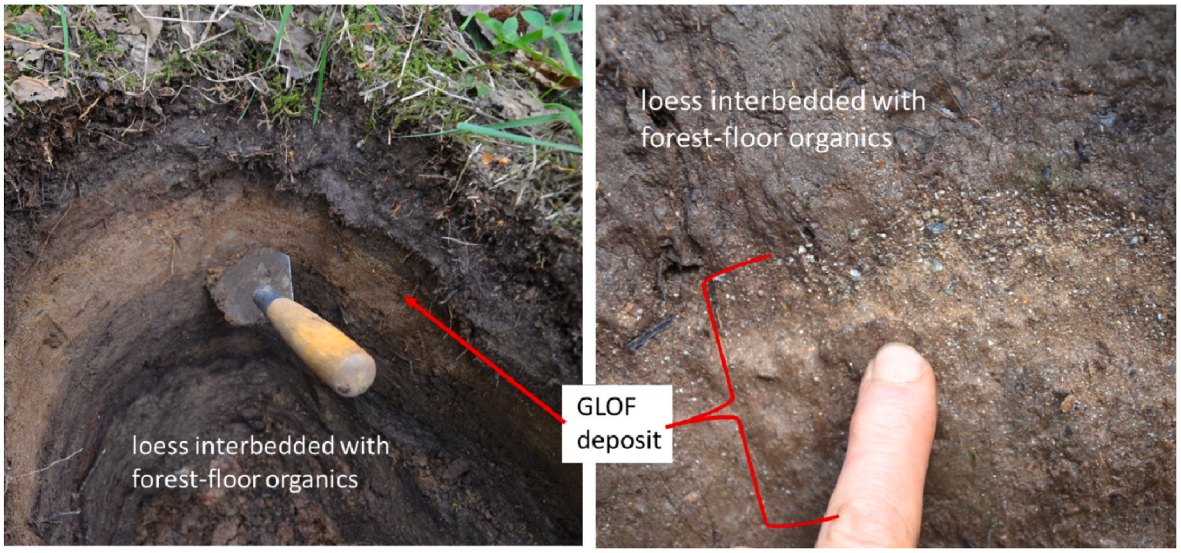

Fig. 13. Soil pits dug on the Lower Fan expose a layer of flood sediment that thins and fines upslope. The unit is inversely graded, ranging from sandy silt near its base to silty sand with granules and occasional pebbles near its top. This flood layer buried a pre-existing forest composed of young spruce trees.

alluvium is underlain by 60^{+} cm of massively structured, medium and coarse sand overlying an undetermined thickness of sandy, boulder gravel. The pith age of the oldest white spruce (AD 1733) growing on the pendant bar in the Northern Kettle Field provides a minimum-limiting age for its formation of ca. AD 1713.

The GLOF that formed the Northern Kettle Field lapped onto the surface of the Lower Fan. Along the low (~3 m) escarpment separating the Lower Fan from the kettle field (Fig. 12), a 5-10 cm layer of silt, sand, granules, with occasional small pebbles buried the pre-existing forest floor. This deposit thins and becomes finer grained upslope across the surface of the Lower Fan (Fig. 13). The unit is inversely graded, perhaps as a result of a surges of hyper-concentrated flood water (Pierson, 1970; Sohn et al., 1999). Some of the spruce trees growing on this surface survived having their roots buried by the flood sediment.

The trees growing on the Lower Fan today provide limiting dates on the GLOF. Of the eleven trees excavated (Fig. 14), six were rooted above the flood deposit, and the oldest of these had a pith date of AD 1714. Five of the excavated trees were rooted below the flood deposit, and the youngest of these had a pith date of AD 1636. Because these dates come from near the tree's root crown, we do not subtract 20 years to account for ecesis. More precise information about the timing of the flood comes from the dendrochronology of the trees that survived the flood (Section

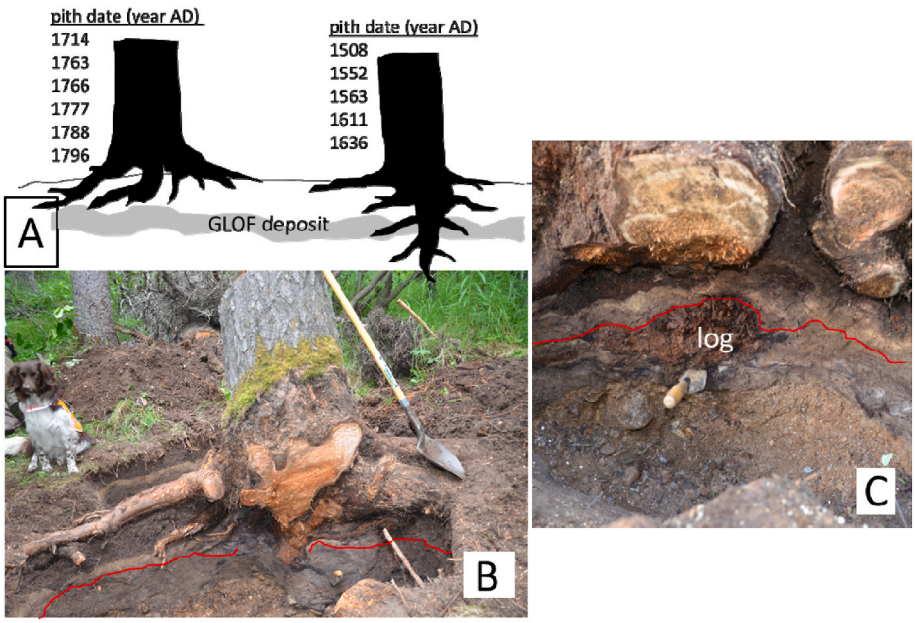

Fig. 14. Excavations of white spruce trees growing on the Lower Fan provide limiting age estimates for the flood that formed the Northern Kettle Field. Red lines trace the base of the flood sand. **A.** Six of the trees were rooted above the layer of flood sand, and the oldest of these had a pith date of AD 1714. Five of the excavated trees were rooted below the sand layer, and the youngest of these had a pith date of AD 1636. **B.** A tree that was a sapling when the flood occurred and is rooted below the flood deposit. Because of cooling soil temperatures and accumulating loess and organic soil horizons, these roots have died and been replaced by roots closer to the ground surface. The pith date of this tree is AD 1508. **C.** The roots of a tree on the Lower Fan that established above the flood sand, which buried a log. The pith date of this tree is AD 1796.

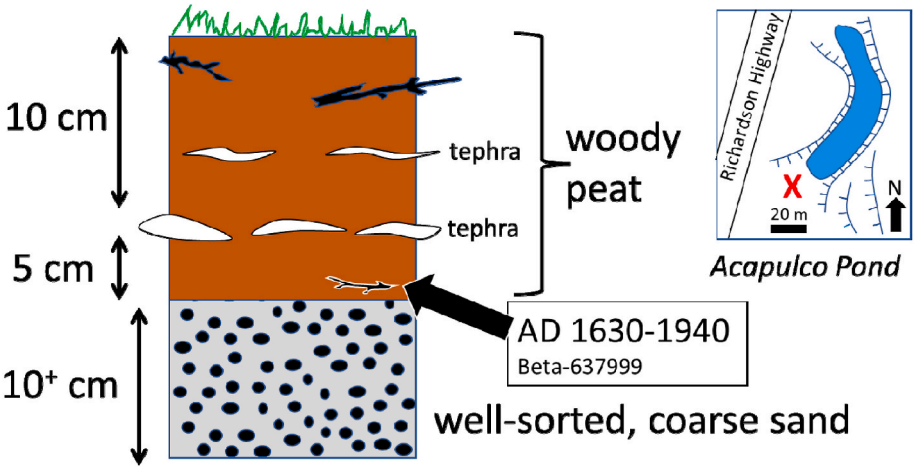

Fig. 15. A twig dating to AD 1630–1940 near the bottom of peat accumulating in a moist hollow provides a minimum-limiting date on when the Delta River abandoned the Acapulco Pond-Rapids Lake-Falls Creek marginal channel.

6.4.1).

6.2.2. Other stratigraphic sections

A 75-cm long piston core from Acapulco Pond yielded a basal date of AD 1670–1950 (Table 3). A 0.5-cm layer of white tephra was present 5 cm above the bottom of the core. A similar tephra layer was present near the base of undated cores retrieved from Rapids Lake. A bedrock hollow near the southern end of Acapulco Lake containing 15 cm of woody peat yielded a twig at the peat/bedrock interface dating to AD 1695–1920 (Fig. 15). Two thin layers of grey tephra were present in this peat accumulation. The oldest tree in the area between Acapulco Pond and lower Tower Road has an uncorrected pith date of AD 1782 (Fig. 2B).

In a road cut bordering the Parks Highway between Acapulco Pond and Camp Terry (Fig. 2), a layer of loess interbedded with organic horizons was buried by indurated till ca. AD 1410–1450. The age of this twig provides a maximum-limiting date on the glacial advance that buried it.

A pit dug in the bottom of a kettle hole in the Eastern Kettle Field (Fig. 16) revealed several layers of forest litter buried by inorganic sediment, mainly loess together with alluvium derived from the nearby alluvial fan. A twig contained in the lowest organic layer yielded a ^{14}C age between AD 1690 and 1870 (Table 3).

The distal portion of Gunnysack Creek's alluvial fan (Fig. 2A) was truncated by the Delta River, possibly during a GLOF (Reger et al., 1993) (Fig. 17). A twig from the base of the loess deposit capping the fan near the driveway leading to the new Black Rapids Lodge yielded a date of 5330–5580 cal yr BP. South of Gunnysack Creek where its alluvial fan is exposed near Camp Terry, charcoal fragments near the base of the capping loess unit date to 2370–2700 cal yr BP (Beta-477317) (Table 3).

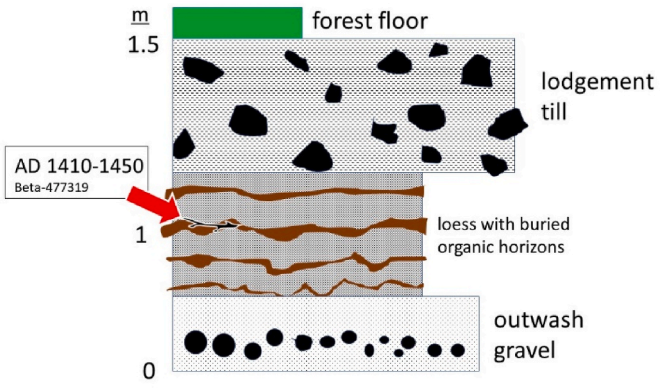

Fig. 16. The "Highway Section" exposed in a road cut along the Richardson Highway between Acapulco Pond and Camp Terry records the burial of a forest soil by till.

6.3. Lichenometric dating

We measured 50 to 240 lichens on each geomorphic surface investigated. The probability of encountering a lichen larger than any previously encountered on same surface declined to <0.05 before 50 lichens were measured (Fig. 18). This indicates that a sample size of n = 50 or greater is likely to include lichens as large as any encountered in larger samples sizes.

The age-calibration curve is based on the diameters of lichens growing on six surfaces of known age (Table 4). The date when the granite block comprising the Richardson Memorial was placed at Isabel Pass (AD 1932) is shown on its affixed plaque. Isabel Pass is located 40 km south of the BRG terminus. The age of the 1936-7 Moraine is known from historical records. The age of the youngest Little Ice Age moraine of the Canwell Glacier (Fig. 1) is based on two white spruce trees that were damaged during the moraine's emplacement (Section 6.4.2). The date when the Amphibolite Knob and the Westside Slabs became subaerial is based on the age of the AD 1703-4 GLOF (Section 6.2.1 and 6.4.1), which marked cessation of flow through the Acapulco Pond-Rapids Lake-Falls Creek marginal channel. The age of the Blue Moraine comes from the date (AD 1665 minus 10 years to account for lake filling) when spruce trees were drowned by the rising waters of Lower Glacial Lake Whistler.

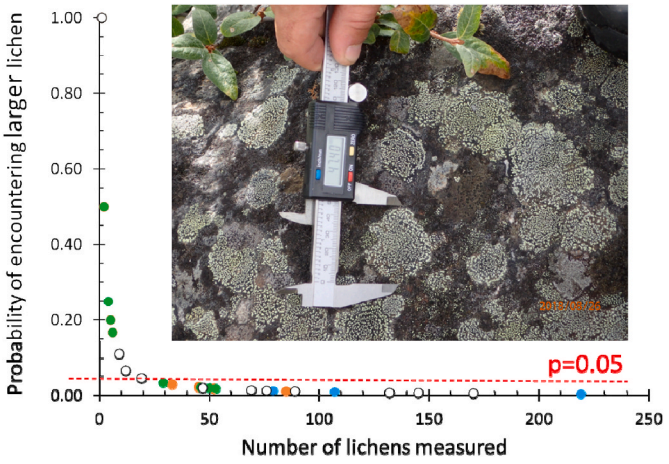

Fig. 18. There is a high probability of encountering the largest lichen among the first 50 lichens measured. Shown here is the declining probability of encountering a lichen larger than any previously measured at the site being examined. Colors correspond to the Green, Blue, and Brown Moraines, with the 1936-7 Moraine shown by open circles. Some data points overlap.

Based on the lichen age-calibration curve (Fig. 19), the Brown Moraine was constructed ca. AD 1866 and the Green Moraine ca. 1488 (Table 5); however, we give little credence to these absolute age estimates. Instead, lichenometric data is most useful for establishing relative ages, correlating between different geomorphic surfaces, and substantiating other age controls. No prediction intervals are given for the age-calibration curve because the lichen diameters on the Green Moraine slightly exceed the age-calibration data. Instead, we apply the ±20% error estimate suggested by Wiles et al. (2010). The resulting age ranges of the Brown and Blue Moraines span 70–210 years. Fortunately, lichenometry-based age estimates are narrowed considerably by the limiting dates provided by dendrochronology and the ^{14}C-dated stratigraphy, together with constraints based on the superposition of moraines (Section 7.1).

6.4. Dendrochronological records of glacial microclimates related to surges and GLOFs

The tree-ring record for the Lower and Upper Alluvial Fan sites Fan is based on 44 trees, the oldest of which has a pith date of AD 1507

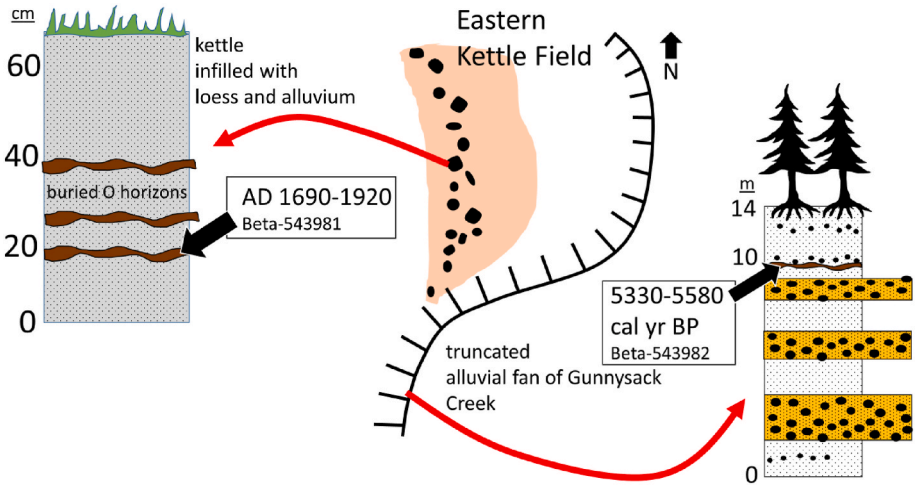

Fig. 17. The ^{14}C age of a buried organic soil horizon in a kettle provides a minimum-limiting age on when the Eastern Kettle Field was deposited. A closer minimum age comes from the oldest tree in the area (AD 1782). Twigs near the base of the loess unit capping the Gunnysack Creek alluvial fan provide a minimum-limiting age on when this portion of the fan was constructed and a maximum-limiting age on when the distal portion of the fan was truncated, possibly by a GLOF. The yellow units in the diagram contain boulder gravel.

Table 4
Independently dated surfaces with measured *Rhizocarpon geographicum*.

Location	Event dated	Dating method	Average of five largest lichens' diameters (mm)	Standard deviation (mm)	Independent age estimate (years)
moraine of BRG	moraine establishment after 1936-7 surge	historical record	24.2	2.0	**82**
Richardson Monument, Isabel Pass	erection of monument in 1932	historical record	35.4	5.7	**91**
youngest Little Ice Age moraine of Canwell Glacier	moraine establishment	dendrochronology of two trees damaged during moraine emplacement	49.0	3.0	**176**
Amphibolite Knob	cessation of flow through the Rapids Lake marginal channel	timing of GLOF recorded by dendrochronology at the Lower and Upper alluvial fans of One Mile Creek	63.6	1.5	**317**
Blue Moraine	damming of Delta River by the Blue Moraine	^{14}C dating and dendrochronology of spruce tree buried in Whistler Creek Delta	63.8	8.1	**337**
Westside Slabs, Falls Creek	cessation of flow through the Rapids Lake marginal channel	timing of GLOF recorded by dendrochronology at the Lower and Upper alluvial fans of One Mile Creek	63.9	2.3	**319**

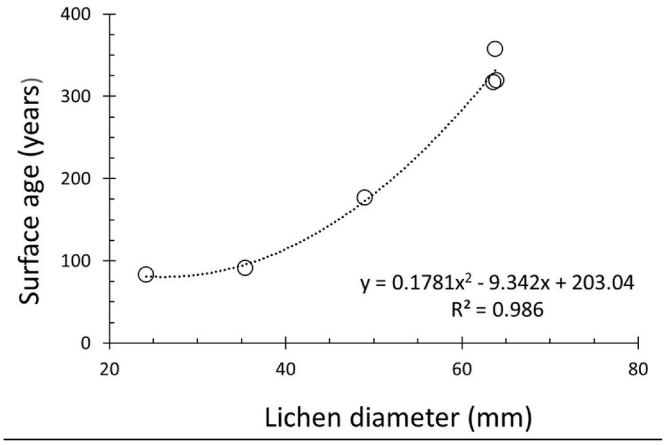

Fig. 19. The relationship between *Rhizocarpon geographicum* diameters and known surface ages in the Black Rapids area. See the text and Table 4 for a description of these control sites.

(Fig. 20). Fourteen trees were sampled on the pendant bar in the Northern Kettle Field (Figs. 9–11), the oldest of which has a pith date of AD 1733, which provides a minimum-limited date on the AD 1703-4 GLOF. The tree-ring record from the area between Acapulco Pond and lower Tower Road is based on 26 trees, the oldest of which has a pith date of AD 1782, which provides a minimum-limiting date on the construction of the Blue Moraine (Fig. 2b). The outer rings of the two spruce stumps buried in the Whistler Creek Delta (Fig. 8) provide a close limiting date on when Lower Glacial Lake Whistler was filled (ca. AD 1677), which is also a minimum-limiting date on the Blue Advance that dammed the lake (ca. AD 1677 minus ~10 years).

Periods of growth divergence between white spruce trees near the BRG help to constrain the timing of glacier surges and GLOFs. The RWIs of white spruce trees growing near the BRG are positively correlated with those from the Wrangell Mountains and Central (Interior) Alaska (Davi et al., 2003; D'Arrigo et al., 2016) (correlations: 0.31, and 0.45, respectively); however, there were several intervals when tree growth in the Black Rapids area diverged from the Wrangell and Interior Alaska chronologies (Fig. 21). Some of these negative divergences represent localized responses to cooling in the Black Rapids area caused by the proximity of the glacier, its proglacial lake, and icebergs stranded after GLOFs. These local events did not affect spruce trees growing in Interior Alaska or in the Wrangell Mountains. Positive divergences from the regional records probably represent stand-level growth releases in the aftermath of widespread tree mortality/damage during episodes of glaciogenic cooling.

A sudden, pronounced, and brief decrease in tree growth began in AD 1703-4 at the Lower and Upper sites on the alluvial fan of One Mile Creek (Fig. 22). Because the regional white spruce chronologies do not exhibit similar slow-downs in growth at this time, we interpret this 1703-4 event as a local response to the GLOF that created the Northern Kettle Field and stranded large numbers of icebergs within 100 m of these trees. Limiting dates from the trees at the Lower Fan Site that are rooted above and below the sediment deposited by this flood are consistent with its occurrence in AD 1703-4 (Section 6.2.1, Fig. 14). Also consistent with the AD 1703-4 date for this GLOF, is the AD 1733 (uncorrected for ecesis) pith date of the oldest tree growing in the Northern Kettle Field (Fig. 12).

Trees near Acapulco Pond experienced an extended interval of reduced growth beginning in AD 1825 that was divergent from the regional RWI records (Fig. 21). We suspect this slow-down in growth near Acapulco Pond began as a response to a cooler microclimate in the Black Rapids foreland caused by the Brown Advance.

6.5. *Dating the youngest Little Ice Age Moraine of the Canwell Glacier*

The search for geomorphic surfaces of known age that would be useful for constructing the lichen age-calibration curve led us to the Canwell Glacier (Figs. 1 and 6) where we found two spruce trees that survived partial burial in the toe of the youngest Little Ice Age Moraine identified by Péwé and Reger (1983). Tree "*6September2022#4*" began forming compression wood in the AD 1846 growing season, indicating that it was tilted by the encroaching moraine shortly before that (Fig. 23a). Tree "*7September2022#1*" was partially buried by the same moraine and then injured by rockfall. The growth of this tree began to

Table 5
Predicted ages of unknown surfaces based on lichenometry.

Site	Diameter of 5 largest lichens (mm)	Standard deviation (mm)	Predicted age (yrs)	Predicted age (year AD)	Minus (plus) 20% of predicted age (year AD)
Brown Moraine	**46.4**	**1.9**	**153**	**1866**	**1835 (1895)**
Green Moraine	**76.6**	**8.1**	**532**	**1487**	**1380 (1590)**

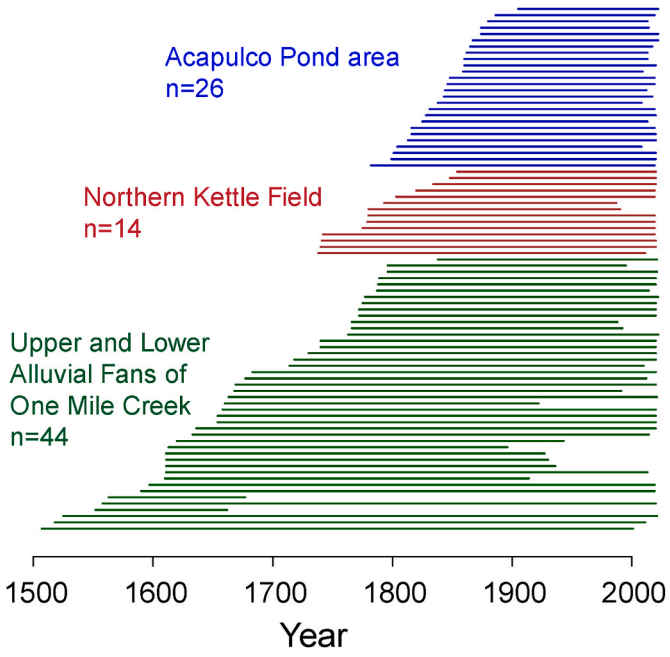

Fig. 20. Tree-ring segment plot for the Black Rapids area.

slow in AD 1843-4. Boulders tumbling down the moraine in AD 1847-8 left a prominent scar on the uphill side of the trunk, and the tree began to lean around that same time (Fig. 23b). These limiting dates of AD 1843–1848 on construction of the youngest Little Ice Age Moraine of the Canwell Glacier are similar to Péwé and Reger's (1983) estimate of AD 1829 based on tree ages; they are also close to Howley's (2008) estimate of AD 1834–1842 for construction of the youngest Little Ice Age moraine of the Castner Glacier.

7. Discussion

7.1. Chronological synthesis

The timing of recent surges by the BRG emerges from a synthesis of data from geomorphology, stratigraphy, lichenometry, radiocarbon dating, and dendrochronology. (Figs. 24 and 25). Four moraines are preserved on the foreland of the BRG (Fig. 2A), and their spatial relationships constrain their order of establishment. Predictably this moraine-based record is incomplete and fades rapidly into the past (Gibbons et al., 1984). Additional surges undoubtedly occurred, but evidence for them has been effaced by larger and/or more recent surges.

The wide uncertainties in lichen-age estimates (Table 4) are narrowed by geomorphic relationships, ^{14}C dates, tree ages, and limiting dates on the formation and drainage of Lower Glacial Lake Whistler (Fig. 24). The lichenometry estimate for the age of the Brown Moraine is AD 1866 within a ±20% error envelope of 1835–1895 (Table 5). Its minimum age is constrained by the AD 1851 pith date (AD. 1871 minus 20 years for ecesis) of the oldest tree found growing on this moraine (Péwé and Reger, 1983; Reger et al., 1993). A closer, maximum-limiting age on the Brown Moraine can be inferred from the tree-ring record. Comparison between the trees growing near Acapulco Pond and those 5.5 km away at the Upper and Lower fan sites reveals a reduction in growth near Acapulco Pond beginning in AD 1825 (Figs. 21 and 24). When the Brown Moraine was constructed, the trees near Acapulco Pond were located <500 m from the glacier terminus. Judging from similar, periglacial situations (Gaglioti et al., 2022, 2024), a cooling of microclimate resulting from the proximity of the glacier probably reduced tree growth near Acapulco Pond. Based on these limiting ages, the surge that constructed the Brown Moraine occurred between AD 1825 and 1851.

The Blue Moraine was constructed prior to the maximum-limiting age of the Brown Moraine (ca. AD, 1825) (Fig. 24). No trees grew close enough to the Blue Moraine to respond to the microclimatic effects of the surge that constructed it; the trees on the alluvial fan of One Mile Creek at the Upper and Lower Fan sites were >2 km away at that time. A minimum-limiting date for construction of the Blue Moraine comes from damming of Lower Glacial Lake Whistler, which drowned trees at the site of the Whistler Creek Delta ca. AD 1677 (Fig. 8, Table 3). Assuming that a decade was required to fill Lower Glacial Lake Whistler, the Blue Moraine was constructed ca. AD 1667. A minimum-limiting date for the

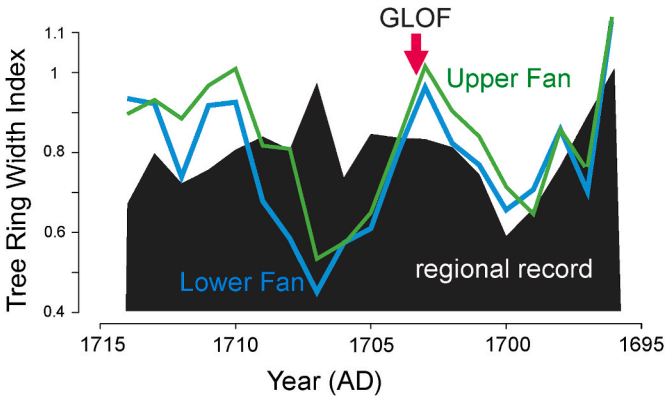

Fig. 22. The effects of a GLOF from Lower Glacial Lake Whistler on tree growth at the Lower Alluvial Fan site (blue line) and the Upper Alluvial Fan site (green line) become evident when compared to the growth of trees in the Wrangell Mountains (black polygon; D'Arrigo et al., 2006). Much of the impact of the GLOF probably resulted from cool summer temperatures caused by large numbers of icebergs scattered across the adjacent floodplain of the Delta River (Section 6.2.1).

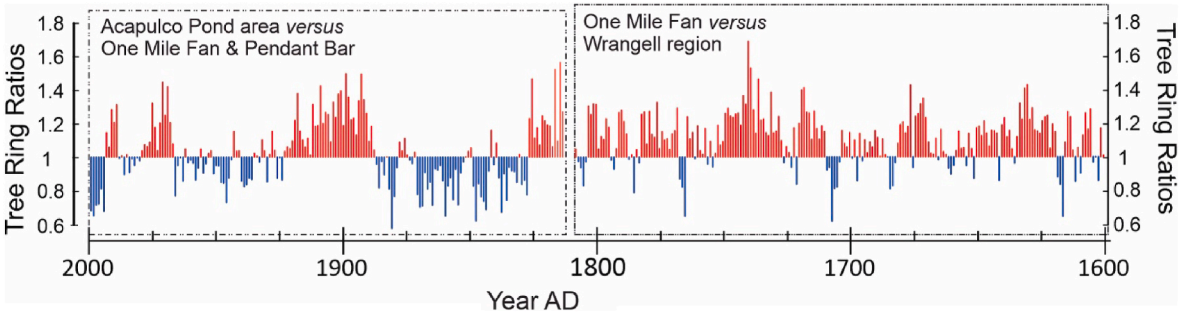

Fig. 21. Ring-width ratios <1 (blue histograms) indicate that tree growth is slower than in the control population. Red histograms indicate the opposite. Between AD 1600 and 1800, the closest trees to the BRG were 1.5 km away at the Lower and Upper sites on the alluvial fan of One Mile Creek. The growth of these trees is compared to trees in the Wrangell Mountains. After AD 1800, trees colonized the area around Acapulco Pond closer to the glacial foreland. The growth of these Acapulco Pond trees is compared to the control provided by trees growing at the Upper and Lower Fan sites.

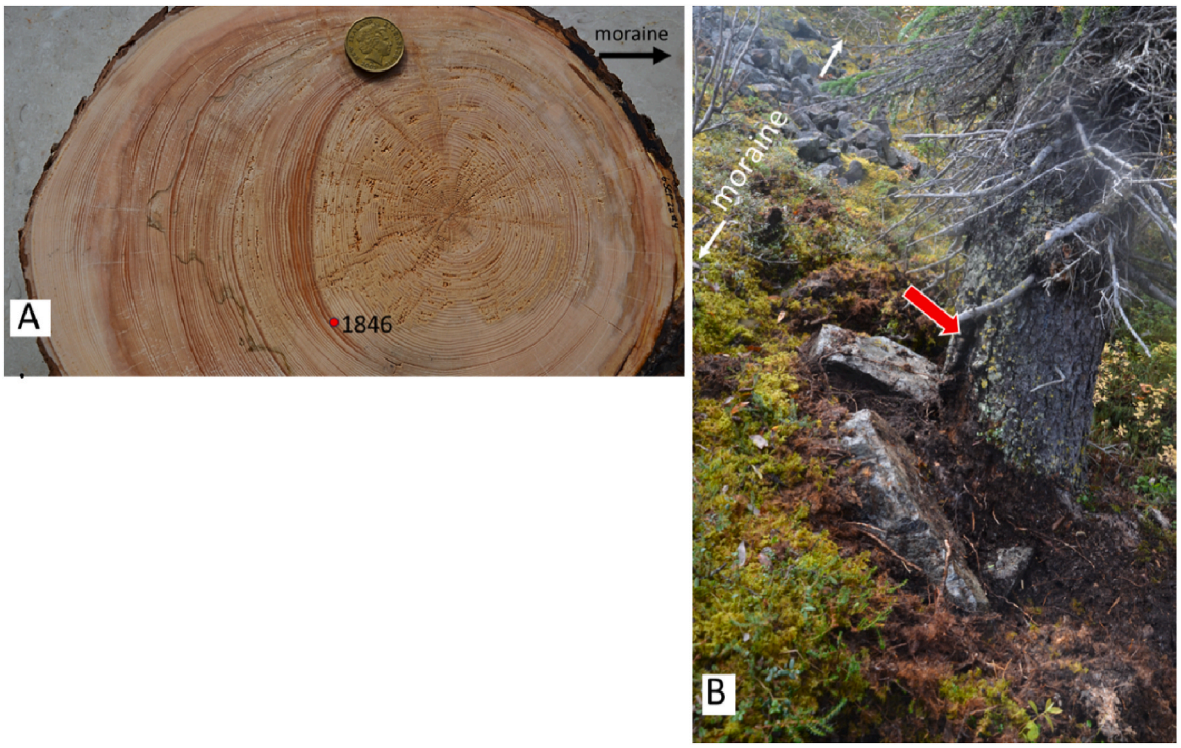

Fig. 23. Damaged trees date the construction of the youngest Little Ice Age moraine of the Canwell Glacier. **A.** Tree "6Sept 2022#4" was partially buried and tilted by construction of the moraine. **B**. Tree "7Sept2022#1" was partly buried, tilted, and then scarred by rockfall.

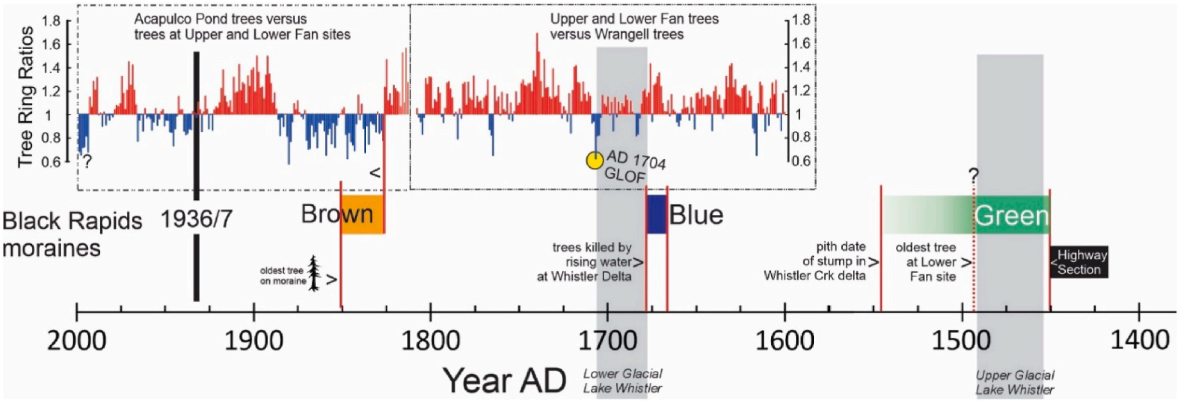

Fig. 24. Chronological synthesis of recent surges of the BRG. The black, vertical line indicates the AD 1936-7 surge.

Blue Moraine comes from the 1703-4 GLOF (Section 6.2.1), which resulted in the emptying of Lower Glacial Lake Whistler and the abandonment of the Acapulco Pond-Rapids Lake-Falls Creek marginal channel. If these dates are correct, Lower Lake Whistler existed for some 26 years, which is plausible given the large amount of rock debris that would have been available to create a dam, and also because the Delta River occupied a stable diversion channel cut into bedrock along the eastern valley wall during that time.

The Green Moraine is estimated by lichenometry to have been constructed between AD 1380 and 1590. A closer, minimum-limiting age comes from the pith date of AD 1532 (AD 1552 minus 20 years for ecesis) of Stump B in the Whistler Creek Delta (Fig. 8). This tree could not have begun growth until after Upper Glacial Lake Whistler drained. The Upper Scour Zone (Fig. 2) resulted from erosion by the Delta River when it was forced against the eastern side of the valley during the Green Advance (Fig. 24); unfortunately, we were unable to find any suitable sites for lichenometry within the Upper Scour Zone.

A closer, minimum-limiting date on the Green Moraine may come from the pith date of the oldest tree at the Lower Fan Site, which is AD 1488 (AD 1508 minus 20 years for ecesis). If Upper Glacial Lake Whistler drained during a large GLOF, it is unlikely that any trees growing at the toe of the alluvial fan of One Mile Creek would have survived. Circumstantial evidence for such GLOF comes from the geomorphology of the Upper and Lower Fan sites (Figs. 9 and 10). As Reger et al. (1993) pointed out, GLOFs probably truncated alluvial fans well above the level of the present floodplain of the Delta River. The northern sector of the Upper Fan was deposited between AD 1270 and 1390 (Fig. 12). Its distal edge was then truncated along a prominent scarp (Fig. 9) now extending several hundred meters to the east of the Northern Kettle Field and standing 4–7 m higher. Sometime before AD 1488 (the ecesis-corrected age of the oldest tree on the Lower Fan), the Upper Fan was incised by the Lower Fan, probably in response to the lowering of local baselevel after a GLOF truncated the Upper Fan. If this scenario is correct, the GLOF responsible for this truncation occurred prior to AD 1488. If this

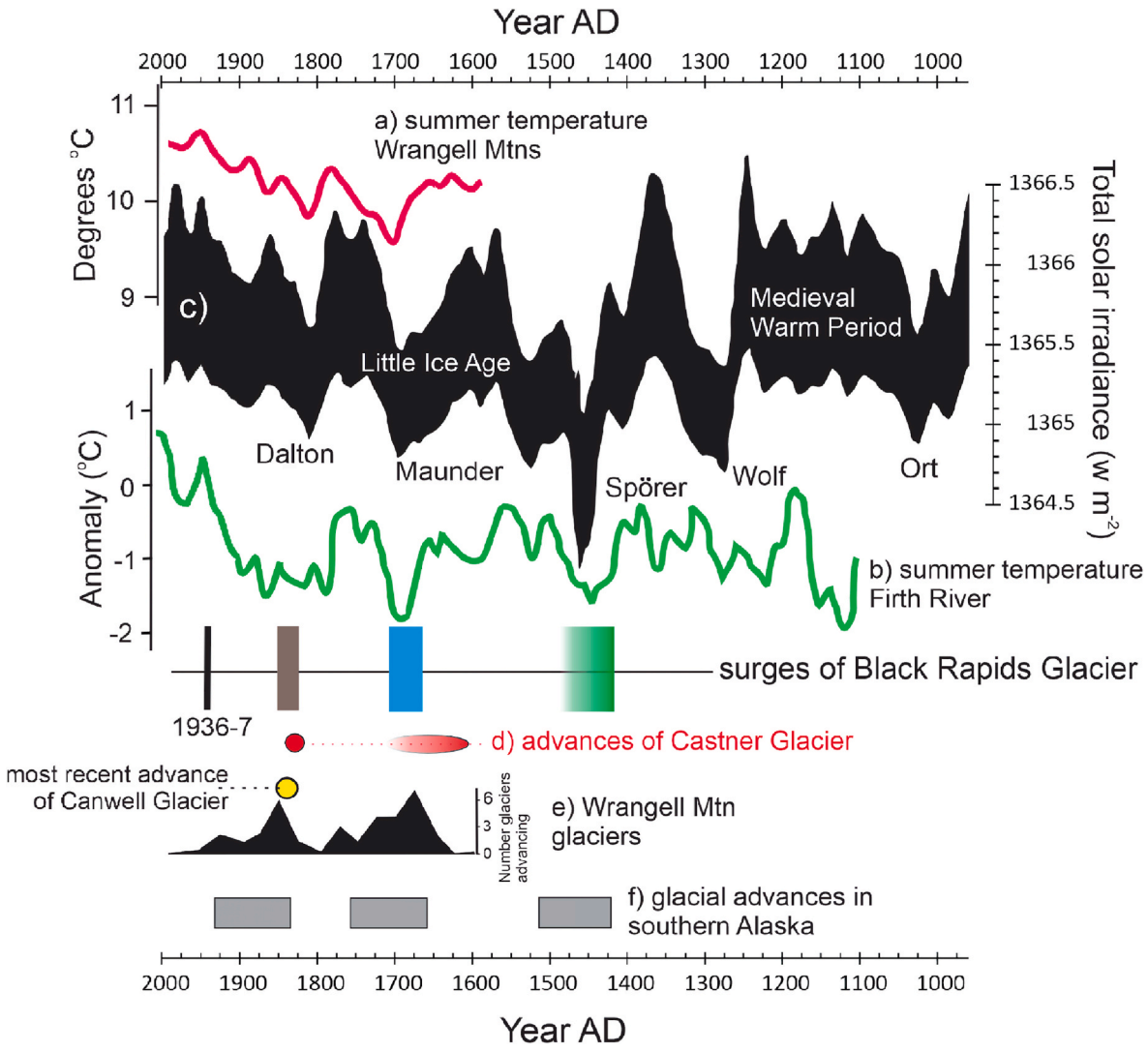

Fig. 25. Between ca. AD 1400 and 1900, the surges of the BRG for which we have records coincided with the advances of non-surging glaciers in the region. The dendrochronological record of summer temperature in the Wrangell Mountains (**a**) is from Davi et al. (2003). The dendrochronological record of summer temperature from the Firth River area in northern Yukon Territory (**b**) is from Anchukaitis et al. (2013). The black polygon (**c**) incorporates the 1-sigma error envelope of solar irradiance associated with the Seuss / de Vries cycle as estimated by Steinhilber and Beer (2011). The recent advances of the Castner Glacier (**d**) were dated by Reger and Péwé (1991) and Howley (2008). The record of glacier fluctuations in the Wrangell Mountains (**e**) is from Wiles et al. (2002, 2004). The times of widespread glacial advances in southern Alaska (**f**) are from Wiles et al. (2008). Other dates are from the present study. Volcanic eruptions in the AD 1450s, 1695, and 1809-10 caused cooling in Alaska and the Yukon (Gao et al., 2008; Davi et al., 2003; Anchukaitis et al., 2013).

GLOF came from Upper Glacial Lake Whistler when it was dammed by the Green Advance, it provides a minimum-limiting date of AD 1488 for that surge (Fig. 24). The dashed vertical line in Fig. 24 reflects the conjectural nature of this reconstruction. A maximum-limiting age for the Green Moraine comes from the Highway Section (Fig. 16 Table 3) where lodgement till buried a soil between AD 1420 and 1450. Taken together, these limiting dates suggest the Green Moraine was constructed sometime between AD 1420 and 1488.

7.2. Geological hazards posed by the BRG

At least twice since AD 1400, the BRG has surged across the Delta River onto terrain where military, highway, and pipeline infrastructure are now located. A major GLOF occurred in AD 1703-4, and an even larger flood probably occurred when Upper Glacial Whistler drained in the late 1400s. These outburst floods from Upper and Lower Glacial Lake Whistler could have had peak discharges exceeding early summer (= peak annual) flows of the Tanana and Yukon Rivers (Table 2). If they occurred today, such floods would cause widespread damage to human infrastructure far downstream.

Fortunately, the BRG now poses few geological hazards because of its increasingly negative mass balance (Larsen et al., 2015; Kienholz et al., 2017), which has removed the possibility of surges crossing the Delta River in the foreseeable future (Heinrichs et al., 1996). A net gain in surface elevation did occur in the glacier's reservoir zone between 1950 and 1995 (Shugar et al., 2010); however, since then the glacier's mass balance has been negative as a result of warmer summers, declining snowfall, and the resultant lowering of the glacier's surface (Kienholz et al., 2017). The landslides triggered by the 2002 Denali Fault Earthquake slowed but did not reverse the BRG's down-wasting trend, and modelling suggests that the BRG will continue retreating over coming decades (Kienholz et al., 2017).

7.3. Responses of the BRG to Little Ice Age climate changes

7.3.1. Regional comparisons

Between AD 1400 and 1900, the surges of the BRG for which we now have records coincided with the advances of non-surging glaciers in the

Table 6
The predicted lag between climate forcing and the responses of seven glaciers in the Wrangell Mountains whose Little Ice Age histories have been documented by Wiles et al. (2002, 2008). The average response time of glaciers in the European Alps that are longer than 1 km is 50 ± 28 years (Zekollari et al., 2020).

Glacier	Length (km)	Slope angle of lowest 80% of length (%)	Elevation range (m)	Predicted response time (years)
Nabesna	70	2.3	2870	38
Nizina	31	3.4	1170	84
Barnard	48	3.6	2800	38
Kennicott	43	3	2930	35
Kuskulana	25	4.9	1700	67
Copper	20	5.6	1544	71
Chisana	36	5.2	2000	59
			Mean	**56**
			Std dev	**19**

region (Fig. 25). As Péwé and Reger (1983) suggested, recent surges of the BRG were coeval with advances of its nearest neighbors, the Castner and Canwell Glaciers, neither of which show clear evidence of being surge-type glaciers. The Brown Surge (AD 1825–1851) was coeval with the youngest Little Ice Age advances of both the Canwell Glacier (AD 1843–1848, Section 6.4.2) and the Castner Glacier (AD 1832–1842; Howley, 2008). Furthermore, our age estimate for the Blue Moraine (AD 1667–1703) overlaps with Howley's (2008) lichenometry-based estimate of AD 1692 for the penultimate advance of the Castner Glacier. Our AD 1667–1703 date nearly overlaps with the cosmogenic ages that Howley (2008) reported from two boulders deposited by that same, penultimate advance of the Castner Glacier (AD 1590–1662).

During the Little Ice Age (ca. AD 1300–1900), the BRG appears to have tracked the same fluctuations in solar irradiance (Wiles et al., 2004) as non-surging glaciers in the region (Fig. 25). On a global basis, solar minima associated with the Seus / de Vries cycle (Lüdecke et al., 2015) probably triggered glacier advances by lowering summer temperature and reducing ablation (Wigley and Kelly, 1990). In the case of the BRG, the Brown Advance occurred during the Dalton Minimum, the Blue Advance during the Maunder Minimum, and the Green Advance during the Spörer Minimum (Fig. 25).

7.3.2. The fading record of surges interferes with estimates of surge-cycle duration

Because older moraines are often destroyed by younger advances (Gibbons et al., 1984; Rowan et al., 2022), the record of the BRG's past surges is incomplete. The probability of missing surges increases with age; even recent surges may be missing from the moraine record if they were less extensive than the 1936-7 surge. We cannot use the glacier's surge cycle to estimate when these missing surges occurred because it is unclear how long the surge cycle of the BRG actually is or how the surge cycle responded to changing climate. Heinrichs et al. (1996) suggested the BRG surges every 50–75 years based on the presence of looped moraines now being pushed out into the main valley by tributary glacier (see Herreid and Truffer (2016) for an illustrated explanation). Under present climatic conditions, the surge cycle is longer than the 88-year time gap between AD 1936 and 2024; however, the present climate is different from that of the Little Ice Age. The interval separating the 1936-37 Surge from the Brown Surge was between 85 and 111 years (Table 5). The interval between the Brown and the Blue surges was 122–184 years, and the interval between the Blue and Green surges was 179–283 years (Fig. 25); however, the latter two intervals are largely irrelevant because of the high probability of missing surges. Based on the interval between the Brown and 1936-37 surges and accepting the reasoning of Heinrichs et al. (1996), the BRG probably had a surge cycle of 80–120 years between the 1600s and 1950. Most of this cycle was occupied by its quiescent phase during which the terminus was stagnant and down-wasting in place.

7.3.3. Why did the BRG fluctuate in synchrony with its non-surging neighbors?

Changes in climate that occur during quiescent phases of an Alaska-type surge cycle are not accompanied by contemporaneous moraine construction at the glacier's terminus. This has important consequences for the geological record because terminal moraines comprise much of that record. Because of its 80- to 120-year surge cycle, some significant events in Little Ice Age climate history may be missing from the moraine record of the BRG. On the other hand, the BRG's recorded surges are concordant with changes in solar irradiance and with the advances of its non-surging neighbors (Fig. 25) Why/how did the BRG track solar irradiance in concert with its non-surging neighbors?

Four phenomena may have contributed to the BRG fluctuating synchronously with non-surging glaciers during the latter part of the Little Ice Age. The first is that non-surging glaciers also have gaps in their geological records, in their case resulting from temporal lags in their responses to climate (Zekollari et al., 2020; Rowan et al., 2022). Among non-surging glaciers in the Wrangell Mountains with known chronologies (Wiles et al., 2002, 2004), these response lags probably ranged from 35 to 84 years (Table 6), which is not significantly shorter than the 80- to 120-year climatically insensitive intervals of the BRG.

Also contributing to the BRG's apparent synchroneity with non-surging glaciers in the region is that only the largest advances/surges are recorded in the moraine records left by any of these glaciers (Gibbons et al., 1984). If we had a record of all the glacier fluctuations that occurred, there might be instances when the BRG responded asynchronously with other glaciers.

It is possible that the BRG's surge cycle was shorter during the Little Ice Age, which then minimized the duration of its quiescent phases and made the glacier more responsive to climate. The BRG's quiescent phases may have decreased to the point where they resembled the climate-response lags of non-surging glaciers in the region (Table 6). The reconstructed chronology of the BRG's surges shows no indication of shortening during the LIA; however, the fading nature of the present record weakens this inference. Note that a shortened surge cycle is not a guaranteed response to a more glaciogenic climatic regime; other surge-type glaciers exhibit a wide range of possible responses to cooling and warming climate (see Section 2.2). Clearly the BRG increased the extent of its surges during the LIA, but it is possible that it retained its 80- to 120-year surge cycle throughout. A more detailed record of surge frequency during the LIA is needed to test this explanation for the synchronicity between the BRG, neighboring glaciers, and the solar cycle.

A process that does not involve shortening of the observed 80- to 120-year surge cycle of the BRG may have contributed to the synchroneity of the BRG with its non-surging neighbors and with the Seuss / de Vries cycle (Lüdecke et al., 2015). The surge cycle of the BRG might itself be the result of long-term tuning by the solar cycle. Perhaps over the course of several millennia (Ma and Vaquero, 2020), successive solar minima in the solar cycle (Fig. 25) partially entrained the BRG's surge cycle. This resulted when quiescent phases that happened to coincide with solar minima were shortened because the glacier's reservoir zone was replenished faster. The opposite occurred when quiescent phases coincided with solar maxima. The net result was to establish the BRG's 80- to 120-year surge cycle and to align it the fluctuations of non-surging glaciers responding to the same solar cycle.

8. Conclusions

A multidisciplinary approach using geomorphology, stratigraphy, lichenometry, radiocarbon dating, and dendrochronology reveals that the Black Rapids Glacier (BRG) in the eastern Alaska Range has experienced at least four surges since AD 1600. Three of these surges crossed the Delta River and overrode the area now occupied by the Richardson Highway and the Trans-Alaska Pipeline. The historically documented 1936-7 surge was less extensive, and the ongoing retreat of the BRG under the present climate makes it unlikely to pose any threat to human

infrastructure. The surge that crossed the Delta River in the late 1600s dammed the upper Delta River valley. This lake drained in an outburst flood in AD 1703-4 that left large icebergs stranded in the valley downstream. Another, even larger outburst flood probably occurred in the AD 1400s. Based on the BRG's recent glaciology and its history over the last several centuries, its surge cycle has varied between 80 and 120 years.

The larger significance of the BRG's history relates to the question of what the glacial geological records of surge-type glaciers say about paleo-climate. The terminus of a surging glacier is where most of its geological records are deposited, but the terminus does not leave a record of climate during the glacier's quiescent phases. Between AD 1400 and 1900, the most extensive surges of the BRG coincided with solar minima in the Seuss / de Vries cycle (Fig. 25). These same solar minima caused non-surging glaciers in the region to advance (Wiles et al., 2004). Given the 80- to 120-year quiescent phases of the BRG, why was there synchroneity between the BRG, solar minima, and non-surging glaciers? We suspect the answer is some combination of the long-term tuning of the BRG's fluctuations by the solar cycle and shortening of the its surge cycle caused by the more glaciogenic conditions of the Little Ice Age that made the climate-response time of the BRG similar to the response times of non-surging glaciers in the region. As a result, geological deposits left by the BRG provide a surprisingly dependable record of regional climate over the last 600 years.

Declaration of competing interest

The authors declare that they have no known competing financial interests or personal relationships that could have appeared to influence the work reported in this paper.

Data availability

Data will be made available on request.

Acknowledgements

Owen Kahn, Molly Yazwinski, and Mary Webb provided able field assistance. We thank Richard Reger, Harold Lovell, and Wes Farnsworth for thoughtful reviews of earlier drafts of this manuscript. Dortchen and Elsie Groves provided bear protection. P.R.W. received support from the UAF Undergraduate Research & Scholarly Activity Program. D.H.M. and B.V.G received support from National Science Foundation grants 2002561, 2124824, and 2131691. M.E.Y. received support from the UAF Water and Environmental Research Center, the U.S. Geological Survey, the Alfred P. Sloan Foundation, and the Choctaw Nation. We thank Annie Hopper of The Lodge at Black Rapids for her hospitality and interest. Michael Lilly of Geo-Watersheds Scientific lent us field equipment and gave P.R.W. time off to work on this project.

References

Allen, S.K., Sattar, A., King, O., Zhang, G., Bhattacharya, A., Yao, T., Bolch, T., 2022. Glacial lake outburst flood hazard under current and future conditions: worst-case scenarios in a transboundary Himalayan basin. Nat. Hazards Earth Syst. Sci. 22, 3765–3785.

Amand, P.S., 1957. Geological and geophysical synthesis of the tectonics of portions of British Columbia, the Yukon Territory, and Alaska. Geol. Soc. Am. Bull. 68, 1343–1370.

Anchukaitis, K.J., D'Arrigo, R.D., Andreu-Hayles, L., Frank, D., Verstege, A., Curtis, A., Buckley, B.M., Jacoby, G.C., Cook, E.R., 2013. Tree-ring-reconstructed summer temperatures from northwestern North America during the last nine centuries. J. Clim. 26, 3001–3012.

Barrand, N.E., Murray, T., 2006. Multivariate controls on the incidence of glacier surging in the Karakoram Himalaya. Arctic Antarct. Alpine Res. 38, 489–498.

Bazai, N.A., Cui, P., Liu, D., Carling, P.A., Wang, H., Zhang, G., Li, Y., Hassan, J., 2022. Glacier surging controls glacier lake formation and outburst floods: the example of the Khurdopin Glacier, Karakoram. Global Planet. Change 208, 103710.

Benedict, J.B., 2009. A review of lichenometric dating and its applications to archaeology. Am. Antiq. 74, 143–172.

Benedict, J.B., 2008. Experiments on lichen growth, III. The shape of the age-size curve. Arctic Antarct. Alpine Res. 40, 15–26.

Benedict, J.B., 1990. Winter frost injury to lichens: Colorado Front Range. Bryologist 423–426.

Benediktsson, Í.Ö., Ingolfsson, O., Schomacker, A., Kjaer, K.H., 2009. Formation of submarginal and proglacial end moraines: implications of ice-flow mechanism during the 1963–64 surge of Brúarjökull. Iceland. Boreas 38, 440–457.

Benediktsson, I.O., Schomacker, A., Johnson, M.D., Geiger, A.J., Ingólfsson, Ó., Guðmundsdóttir, E.R., 2015. Architecture and structural evolution of an early Little Ice Age terminal moraine at the surge-type glacier Múlajökull, Iceland. Journal of Geophysical Research Earth Surface Processes 120, 1895–1910. https://doi.org/10.1002/2015JF003514.

Ben-Yehoshua, D., Aradóttir, N., Farnsworth, W., Benediktsson, I., Ingólfsson, O., 2023. Formation of crevasse-squeeze ridges at Trygghamna, Svalbard. Earth Surf. Process. Landforms 48, 1–15.

Benn, D.I., Fowler, A., Hewitt, I., Sevestre, H., 2019. A general theory of glacier surges. J. Glaciol. 65, 701–716.

Benn, D.I., Hewitt, I.J., Luckman, A.J., 2022. Enthalpy balance theory unifies diverse glacier surge behaviour. Ann. Glaciol. 63 (87–89), 88–94.

Bevington, A., Copland, L., 2014. Characteristics of the last five surges of Lowell Glacier, Yukon, Canada, since 1948. J. Glaciol. 60, 113–123.

Bhambri, R., Hewitt, K., Kawishwar, P., Kumar, A., Verma, A., Tiwari, S., Misra, A., others, 2019. Ice-dams, outburst floods, and movement heterogeneity of glaciers. Karakoram. Global and Planetary Change 180, 100–116.

Bhambri, R., Hewitt, K., Kawishwar, P., Pratap, B., 2017. Surge-type and surge-modified glaciers in the Karakoram. Sci. Rep. 7, 15391.

Bieniek, P.A., Walsh, J.E., Fresco, N., Tauxe, C., Redilla, K., 2022. Anticipated changes in Alaska extreme precipitation. J. Appl. Meteorol. Climatol. 61, 97–108.

Björnsson, H., 1992. Jokulhlaups in Iceland: prediction, characteristics and simulation. Ann. Glaciol. 16, 95–106.

Bradwell, T., 2009. Lichenometric dating: a commentary, in the light of some recent statistical studies. Geografiska Annaler: series A. Phys. Geogr. 91, 61–69.

Brynjólfsson, S., Schomacker, A., Ingólfsson, O., Keiding, J.K., 2015a. Cosmogenic 36Cl exposure ages reveal a 9.3 ka BP glacier advance and the Late Weichselian-Early Holocene glacial history of the Drangajökull region, northwest Iceland. Quat. Sci. Rev. 126, 140–157.

Brynjólfsson, S., Schomacker, A., Guðmundsdóttir, E.R., Ingólfsson, Ó., 2015b. A 300-year surge history of the Drangajökull ice cap, northwest Iceland, and its maximum during the 'Little Ice Age'. Holocene 25, 1076–1092.

Bunn, A.G., 2008. A dendrochronology program library in R (dplR). Dendrochronologia 26, 115–124.

Burke, M.J., Woodward, J., Russell, A.J., 2010. Sedimentary architecture of large-scale, jökulhlaup-generated, ice-block obstacle marks: examples from Skeiðarársandur, SE Iceland. Sediment. Geol. 227, 1–10.

Carrivick, J.L., Tweed, F.S., 2019. A review of glacier outburst floods in Iceland and Greenland with a megafloods perspective. Earth Sci. Rev. 196, 102876.

Carswell, 2013. The 3D elevation program—summary for Alaska: U.S. Geological Survey fact sheet. 2013–3083. https://pubs.usgs.gov/fs/2013/3083.

Clague, J.J., Mathews, W.H., 1973. The magnitude of jökulhlaups. J. Glaciol. 12, 501–504.

Clague, J.J., O'Connor, J.E., 2021. Glacier-related outburst floods. In: Snow and Ice-Related Hazards, Risks, and Disasters. Elsevier, pp. 467–499.

Clarke, G.K., Schmok, J.P., Ommanney, C.S.L., Collins, S.G., 1986. Characteristics of surge-type glaciers. J. Geophys. Res. Solid Earth 91, 7165–7180.

Cook, S.J., Christoffersen, P., Truffer, M., Chudley, T.R., Abellan, A., 2021. Calving of a large Greenlandic tidewater glacier has complex links to meltwater plumes and mélange. J. Geophys. Res.: Earth Surf. 126.

Copland, L., Sylvestre, T., Bishop, M.P., Shroder, J.F., Seong, Y.B., Owen, L.A., Bush, A., Kamp, U., 2011. Expanded and recently increased glacier surging in the Karakoram. Arctic Antarct. Alpine Res. 43, 503–516.

Costa, J.E., 1988. Rheologic, geomorphic and sedimentologic differentiation of water floods, hyperconcentrated flows and debris flows. Flood Geomorphology 113–122.

Costa, J.E., 1985. Floods from dam failures. US Geological Survey Publication 85, 54.

D'Arrigo, R., Wilson, R., Jacoby, G., 2006. On the long-term context for late twentieth century warming. J. Geophys. Res.: Atmospheres 111. https://doi.org/10.1029/2005JD006352.

Davi, N.K., Jacoby, G.C., Wiles, G.C., 2003. Boreal temperature variability inferred from maximum latewood density and tree-ring width data, Wrangell Mountain region, Alaska. Quaternary Research 60, 252–262.

Dowdeswell, J.A., Hamilton, G.S., Hagen, J.O., 1991. The duration of the active phase on surge-type glaciers: contrasts between Svalbard and other regions. J. Glaciol. 37, 388–400.

Dowdeswell, J.A., Hodgkins, R., Nuttall, A.M., Hagen, J.O., Hamilton, G.S., 1995. Mass balance change as a control on the frequency and occurrence of glacier surges in Svalbard, Norwegian High Arctic. Geophys. Res. Lett. 22, 2909–2912.

Du, J., Zhou, G.G., Tang, H., Turowski, J.M., Cui, K.F., 2023. Classification of stream, hyperconcentrated, and debris flow using dimensional analysis and machine learning. Water Resour. Res. 59, E2022WR033242.

Dunse, T., Schellenberger, T., Hagen, J., 2015. Glacier-surge mechanisms promoted by a hydro-thermodynamic feedback to summer melt. Cryosphere 9, 197–215.

Eisen, O., Harrison, W.D., Raymond, C.F., Echelmeyer, K.A., Bender, G.A., Gorda, J.L., 2005. Variegated Glacier, Alaska, USA: a century of surges. J. Glaciol. 51, 399–406.

Ellis, J.M., Calkin, P.E., 1984. Chronology of Holocene glaciation, central Brooks range, Alaska. Geol. Soc. Am. Bull. 95, 897–912.

Evans, D.J., Rea, B.R., 1999. Geomorphology and sedimentology of surging glaciers: a land-systems approach. Ann. Glaciol. 28, 75–82.

Evans, D.J., Storrar, R.D., Rea, B.R., 2016. Crevasse-squeeze ridge corridors: diagnostic features of late-stage palaeo-ice stream activity. Geomorphology 258, 40–50.
Farnsworth, W.R., Ingólfsson, Ó., Retelle, M., Schomacker, A., 2016. Over 400 previously undocumented Svalbard surge-type glaciers identified. Geomorphology 264, 52–60. https://doi.org/10.1016/j.geomorph.2016.03.025.
Fowler, A., 1987. A theory of glacier surges. Journal of Geophysical Research: Solid Earth 92, 9111–9120.
Gaglioti, B.V., Mann, D.H., Wiles, G.C., 2022. Ecosystems at glacier margins can serve as climate-change laboratories. Geophys. Res. Lett. 49.
Gaglioti, B.V., Mann, D.H., Wiles, G.C., Andreu-Hayles, L., Hansen, W.D., Wiesenberg, N., 2024. Forest-wide growth rates stabilize after experiencing accelerated temperature changes near an Alaskan glacier. Geophys. Res. Lett. 51. https://doi.org/10.1029/2024GL109469.
Gao, C., Robock, A., Ammann, C., 2008. Volcanic forcing of climate over the past 1500 years: an improved ice core-based index for climate models. J. Geophys. Res. Atmos. 113, D23111.
Geist, O., Péwé, T., 1957. Quantitative measurements of the 1937 advance of the BRG, Alaska. Proceedings of the Fifth Alaska Science Conference. Anchorage 1954, 51–52.
Gibbons, A.B., Megeath, J.D., Pierce, K.L., 1984. Probability of moraine survival in a succession of glacial advances. Geology 12, 327–330.
Giddings, J., 1988. Thunder from below—University of Alaska 1937 Black Rapids Glacier Expedition. Journal of Northern Science 2, 33–39.
Haeberli, W., 1983. Frequency and characteristics of glacier floods in the Swiss Alps. Ann. Glaciol. 4, 85–90.
Haeberli, W., Drenkhan, F., 2022. Future lake development in deglaciating mountain ranges. In: Oxford Research Encyclopedia of Natural Hazard Science, Pp. 1–45.
Hamilton, G.S., Dowdeswell, J.A., 1996. Controls on glacier surging in Svalbard. J. Glaciol. 42, 157–168.
Hance, J.H., 1937. The recent advance of Black Rapids Glacier, Alaska. J. Geol. 45, 775–783.
Harrison, W.D., Post, A.S., 2003. How much do we really know about glacier surging? Ann. Glaciol. 36, 1–6.
Hart, J.K., 1995. Subglacial erosion, deposition and deformation associated with deformable beds. Prog. Phys. Geogr. 19, 173–191.
Heinrichs, T.A., Mayo, L., Echelmeyer, K., Harrison, W., 1996. Quiescent-phase evolution of a surge-type glacier: Black Rapids Glacier, Alaska, USA. J. Glaciol. 42, 110–122.
Herreid, S., Truffer, M., 2016. Automated detection of unstable glacier flow and a spectrum of speedup behavior in the Alaska Range. J. Geophys. Res. Earth Surf. 121, 64–81.
Hoinkes, H.C., 1969. Surges of the Vernagtferner in the Ötztal Alps since 1599. Can. J. Earth Sci. 6, 853–861.
Holmes, R.L., 1983. Computer-assisted quality control in tree-ring dating and measurement. Tree-Ring Bull. 43, 51–67.
Howley, M.W., 2008. A late Glacial and Holocene Chronology of the Castner Glacier, Delta River Valley, Alaska. MSc. Thesis. University of New Hampshire, 78 pp.
Huber, M.L., Lupker, M., Gallen, S.F., Christl, M., Gajurel, A.P., 2020. Timing of exotic, far-travelled boulder emplacement and paleo-outburst flooding in the central Himalaya. Earth Surface Dynamics Discussions 2020, 1–29.
Ingólfsson, Ó., 2016. Glacial geological studies of surge-type glaciers in Iceland — Research status and future challenges. Earth Sci. Rev. 152, 37–69.
Jacquemart, M., Cicoira, A., 2022. Hazardous glacier instabilities: ice avalanches, sudden large-volume detachments of low-angle mountain glaciers, and glacier surges. In: Treatise on Geomorphology. Volume 4: Cryospheric Geomorphology. Academic Press, pp. 330–345.
Jiskoot, H., 2011. Glacier surging. In: Encyclopedia of Earth Sciences Series, Pp. 415–428.
Jiskoot, H., Murray, T., Boyle, P., 2000. Controls on the distribution of surge-type glaciers in Svalbard. J. Glaciol. 46, 412–422.
Kamb, B., Raymond, C., Harrison, W., Engelhardt, H., Echelmeyer, K., Humphrey, N., Brugman, M., Pfeffer, T., 1985. Glacier surge mechanism: 1982-1983 surge of Variegated Glacier, Alaska. Science 227, 469–479.
Kienholz, C., Hock, R., Truffer, M., Bieniek, P., Lader, R., 2017. Mass balance evolution of Black Rapids Glacier, Alaska, 1980–2100, and its implications for surge recurrence. Front. Earth Sci. 5, 56. https://doi.org/10.3389/feart.2017.00056.
Kienholz, C., Pierce, J., Hood, E., Amundson, J.M., Wolken, G.J., Jacobs, A., Hart, S., Wikstrom Jones, K., Abdel-Fattah, D., Johnson, C., Conaway, J.S., 2020. Deglacierization of a marginal basin and implications for outburst floods, Mendenhall Glacier, Alaska. Front. Earth Sci. 8, 137. https://doi.org/10.3389/feart.2020.00137.
Kjær, K.H., Larsen, E., Meer, J., 2006. Subglacial decoupling at the sediment/bedrock interface: a new mechanism for rapid flowing ice. Quat. Sci. Rev. 25, 2704–2712.
Kochtitzky, W., Winski, D., McConnell, E., Kreutz, K., Campbell, S., Enderlin, E.M., Copland, L., Williamson, S., Main, B., Jiskoot, H., 2020. Climate and surging of Donjek Glacier, Yukon, Canada. Arctic Antarct. Alpine Res. 52, 264–280.
Koehler, R.D., Carver, G.A., Seismic, Alaska, 2018. Active faults and seismic hazards in Alaska: Alaska Division of Geological & Geophysical Surveys, Miscellaneous Publication. Hazards Safety Commission 160, 59.
Larsen, C., Burgess, E., Arendt, A., O'neel, S., Johnson, A., Kienholz, C., 2015. Surface melt dominates Alaska glacier mass balance. Geophys. Res. Lett. 42, 5902–5908.
Loso, M.G., Doak, D.F., 2006. The biology behind lichenometric dating curves. Oecologia 147, 223–229.
Lovell, H., Fleming, E.J., Benn, D.I., Hubbard, B., Lukas, S., Naegeli, K., 2015. Former dynamic behaviour of a cold-based valley glacier on Svalbard revealed by basal ice and structural glaciology investigations. J. Glaciol. 61, 309–328. https://doi.org/10.3189/2015JoG14J120.
Lovell, H., Carrivick, J.L., King, O., Sutherland, J.L., Yde, J.C., Boston, C.M., Małecki, J., 2023. Surge-type glaciers in Kalaallit Nunaat (Greenland): distribution, temporal patterns and climatic controls. J. Glaciol. 1–18.
Lüdecke, H.-J., Weiss, C.O., Hempelmann, A., 2015. Paleoclimate forcing by the solar De Vries/Suess cycle. Clim. Past Discuss 11, 279–305.
Lützow, N., Veh, G., Korup, O., 2023. A global database of historic glacier lake outburst floods. Earth Syst. Sci. Data Discuss. 2023, 1–27.
Ma, L., Vaquero, J.M., 2020. New evidence of the Suess/de Vries cycle existing in historical naked-eye observations of sunspots. Open Astronomy 29, 28–31.
Maizels, J., 1997. Jökulhlaup deposits in proglacial areas. Quat. Sci. Rev. 16, 793–819.
McCarthy, D.P., 2021. A simple test of lichenometric dating using bidecadal growth of *Rhizocarpon geographicum agg.* and structure-from-motion photogrammetry. Geomorphology 385, 107736.
Meier, M.F., Post, A., 1969. What are glacier surges? Can. J. Earth Sci. 6, 807–817.
Mendenhall, W.C., 1900. A reconnaissance from resurrection bay to the Tanana River, Alaska, in 1898. U.S. Geological Survey 20th Annual Report, pt. 7, pp. 265–340.
Moffit, F.H., 1942. Geology of the Gerstle River District, Alaska and with a report on the Black Rapids Glacier. In: U.S. Geological Survey Bulletin 926, Pp. 107–160.
Moffit, F.H., 1954. Geology of the eastern part of the Alaska Range and adjacent area. In: U.S. Geological Survey Bulletin 989-D, Pp. 65–218.
Murray, T., Strozzi, T., Luckman, A., Jiskoot, H., Christakos, P., 2003. Is there a single surge mechanism? Contrasts in dynamics between glacier surges in Svalbard and other regions. J. Geophys. Res. Solid Earth 108, 2237.
Ng, F., Björnsson, H., 2003. On the Clague–Mathews relation for jökulhlaups. J. Glaciol. 49, 161–172.
Nokleberg, W., Lange, I., Singer, D., Curtin, G., Tripp, R., Campbell, D., Yeend, W., 1990. Metalliferous mineral resource assessment maps of the Mount Hayes quadrangle, eastern Alaska range, Alaska. U.S. Geological Survey Miscellaneous Field Studies Map MF-1996-A, 22 p. 4 sheets, scale 1.
Olszewski, A., Weckwerth, P., 1999. The morphogenesis of kettles in the Hofdabrekkujokull foreland, Myrdalssandur, Iceland. Jokull 47, 71–88.
O'Neal, M.A., Legg, N.T., Hanson, B., Morgan, D.J., Rothgeb, A., 2013. Lichenometric dating of rock surfaces in the northern Cascade Range, USA. Geografiska Annaler: Series A. Phys. Geogr. 95, 241–248.
Osborn, G., McCarthy, D., LaBrie, A., Burke, R., 2015. Lichenometric dating: science or pseudo-science? Quaternary Research 83, 1–12.
Péwé, T.L., 1951. Recent history of Black Rapids Glacier, Alaska. Geol. Soc. America Bull. 62, 1558 (Abstract).
Péwé, T.L., Reger, R.D., 1983. Guidebook to Permafrost and Quaternary geology along the Richardson and Glenn Highways between Fairbanks and Anchorage, Alaska. In: Fourth International Conference on Permafrost, July 18-22, 1983. University of Alaska, Fairbanks, Alaska, USA. Division of Geological & Geophysical Surveys, Department of Natural Resources.
Pierson, T.C., 1970. Hyperconcentrated flow–transitional process between water flow and debris flow. In: Jakob, M., Hungr, O. (Eds.), Debris-Flow Hazards and Related Phenomena. Springer Berlin Heidelberg, pp. 159–202.
Post, A., 1969. Distribution of surging glaciers in western North America. J. Glaciol. 8, 229–240.
Post, A., 1967. Effects of the March 1964 Alaska Earthquake on glaciers. In: U.S. Geological Survey Professional Paper 544D, pp. 1–44.
Post, A., Mayo, L.R., 1971. Glacier dammed lakes and outburst floods in Alaska. In: U.S. Geological Survey Hydrological Investigations Atlas 455, 10 P, 3 Sheets, Scale 1: 1,000,000.
Post, A.S., 1960. The exceptional advances of the Muldrow, Black Rapids, and Susitna glaciers. J. Geophys. Res. 65, 3703–3712.
Raymond, C.F., 1987. How do glaciers surge? A review. Journal of Geophysical Research: Solid Earth 92, 9121–9134.
Rea, B.R., Evans, D.J., 2011. An assessment of surge-induced crevassing and the formation of crevasse squeeze ridges. J. Geophys. Res.: Earth Surf. 116, F4005.
Reger, R.D., Péwé, T.L., 1991. Dating Holocene moraines of Canwell Glacier, Delta River valley, central Alaska range. In: Reger, R.D. (Ed.), Short Notes on Alaskan Geology 1991: Alaska Division of Geological & Geophysical Surveys Professional Report 111H, pp. 63–68. https://doi.org/10.14509/2299.
Reger, R.D., Sturmann, A.G., Begét, J.E., 1993. Dating Holocene moraines of Black Rapids Glacier, Delta River valley, central Alaska Range. Short Notes on Alaskan Geology 113, 51–59.
Reimer, P.J., 2020. Composition and consequences of the IntCal20 radiocarbon calibration curve. Quaternary Research 96, 22–27.
Riehle, J., Fleming, M.D., Molnia, B., Dover, J., Kelley, J.S., Miller, M.L., Nokleberg, W., Plafker, G., Till, A., 1997. Digital shaded-relief image of Alaska. In: U.S. Geological Survey Geological Investigation Series I-2585.
Roof, S., Werner, A., 2011. Indirect growth curves remain the best choice for lichenometry: evidence from directly measured growth rates from Svalbard. Arctic Antarct. Alpine Res. 43, 621–631.
Rosenwinkel, S., Korup, O., Landgraf, A., Dzhumabaeva, A., 2015. Limits to lichenometry. Quat. Sci. Rev. 129, 229–238.
Rowan, A.V., Egholm, D.L., Clark, C.D., 2022. Forward modelling of the completeness and preservation of palaeoclimate signals recorded by ice-marginal moraines. Earth Surf. Process. Landforms 47, 2198–2208.
Russell, A.J., 1993. Obstacle marks produced by flow around stranded ice blocks during a glacier outburst flood (jökulhlaup) in West Greenland. Sedimentology 40, 1091–1111.
Schomacker, A., 2014. The Eyjabakkajökull glacial landsystem, Iceland: geomorphic impact of multiple surges. Geomorphology 218, 98–107.

Sevestre, H., Benn, D.I., 2015. Climatic and geometric controls on the global distribution of surge-type glaciers: implications for a unifying model of surging. J. Glaciol. 61, 646–662.
Sevestre, H., Benn, D.I., Luckman, A., Nuth, C., Kohler, J., Lindbäck, K., Pettersson, R., 2018. Tidewater glacier surges initiated at the terminus. J. Geophys. Res.: Earth Surf. 123, 1035–1051. https://doi.org/10.1029/2017JF004358.
Sharp, M.J., 1985. "Crevasse-fill" ridges—a landform type characteristic of surging glaciers? 1180 Geografiska Annaler: Series A. Phys. Geogr. 67, 213–220.
Sharp, M., 1988. Surging glaciers: behavior and mechanisms. Prog. Phys. Geogr. 12, 349–370.
Shugar, D.H., Rabus, B.T., Clague, J.J., 2010. Elevation changes (1949–1995) of Black Rapids Glacier, Alaska, derived from a multi-baseline InSAR DEM and historical maps. J. Glaciol. 56, 625–634.
Shugar, D.H., Rabus, B.T., Clague, J.J., Capps, D.M., 2012. The response of Black Rapids Glacier, Alaska, to the Denali Earthquake rock avalanches. J. Geophys. Res.: Earth Surface 117. https://doi.org/10.1029/2011jf002011.
Shulski, M., Wendler, G., 2007. The Climate of Alaska. University of Alaska Press.
Sohn, Y.K., Rhee, C.W., Kim, B.C., 1999. Debris flow and hyperconcentrated flood-flow deposits in an alluvial fan, northwestern part of the Cretaceous Yongdong Basin, Central Korea. J. Geol. 107, 111–132.
Solgaard, A., Simonsen, S., Grinsted, A., Mottram, R., Karlsson, N., Hansen, K., Kusk, A., Sørensen, L., 2020. Hagen Bræ: a surging glacier in North Greenland—35 years of observations. Geophys. Res. Lett. 47.
Solomina, O., Calkin, P.E., 2003. Lichenometry as applied to moraines in Alaska, USA, and Kamchatka, Russia. Arctic Antarct. Alpine Res. 35, 129–143.
Steinhilber, F., Beer, J., 2011. Solar activity–the past 1200 years. PAGES News 19, 5–6.
Stokes, M.A., 1996. An Introduction to Tree-Ring Dating. University of Arizona Press.
Stout, J., Brady, J., Weber, F., Page, R., 1973. Evidence for Quaternary movement on the McKinley strand of the Denali Fault in the Delta River area, Alaska. Geol. Soc. Am. Bull. 84, 939–948.
Striberger, J., Björck, S., 2011. Climatic control of the surge periodicity of an Icelandic outlet glacier. J. Quat. Sci. 26, 561–565.
Tarr, R.S., Martin, L., 1914. Alaskan Glacier Studies of the National Geographic Society in the Yakutat Bay, Prince William Sound and Lower Copper River Regions. National Geographic Society.
Terleth, Y., Bartholomaus, T.C., Liu, J., Beaud, F., Mikesell, T.D., Enderlin, E.M., 2024. Transient subglacial water routing efficiency modulates ice velocities prior to surge termination on Sít' Kusá, Alaska. J. Glaciol. 1–17. https://doi.org/10.1017/jog.2024.38.
Trenbirth, H.E., Matthews, J.A., 2010. Lichen growth rates on glacier forelands in southern Norway: preliminary results from a 25-year monitoring programme. Geografiska Annaler: Series A. Phys. Geogr. 92, 19–39.
Truffer, M., 2021. Glacier surges. In: Snow and Ice-Related Hazards, Risks, and Disasters. Elsevier, pp. 417–466.
US Geological Survey National Water Information System. https://waterdata.usgs.gov/nwis/wys_rpt?dv_ts, 2024.
Walder, J.S., Costa, J.E., 1996. Outburst floods from glacier-dammed lakes: the effect of mode of lake drainage on flood magnitude. Earth Surf. Process. Landforms 21, 701–723.
Walder, J.S., O'Connor, J.E., 1997. Methods for predicting peak discharge of floods caused by failure of natural and constructed earthen dams. Water Resour. Res. 33, 2337–2348.
Westoby, M.J., Glasser, N.F., Brasington, J., Hambrey, M.J., Quincey, D.J., Reynolds, J. M., 2014. Modelling outburst floods from moraine-dammed glacial lakes. Earth Sci. Rev. 134, 137–159.
Wigley, T.M., Kelly, P., 1990. Holocene climatic change, ^{14}C wiggles and variations in solar irradiance. Philosophical Transactions of the Royal Society of London. Series A. Mathematical and Physical Sciences 330, 547–560.
Wilbur, S.W., 1988. Surging versus Non-surging Glaciers: a Comparison Using Morphometry and Balance. M.Sc. thesis, University of Alaska Fairbanks.
Wiles, G.C., Barclay, D.J., Calkin, P.E., Lowell, T.V., 2008. Century to millennial-scale temperature variations for the last two thousand years indicated from glacial geologic records of Southern Alaska. Global Planet. Change 60, 115–125.
Wiles, G.C., Barclay, D.J., Young, N.E., 2010. A review of lichenometric dating of glacial moraines in Alaska. Geografiska Annaler: Series A,. Phys. Geogr. 92, 101–109.
Wiles, G.C., D'Arrigo, R.D., Villalba, R., Calkin, P.E., Barclay, D.J., 2004. Century-scale solar variability and Alaskan temperature change over the past millennium. Geophys. Res. Lett. 31, L15203.
Wiles, G.C., Jacoby, G.C., Davi, N.K., McAllister, R.P., 2002. Late Holocene glacier fluctuations in the Wrangell mountains, Alaska. Geol. Soc. Am. Bull. 114, 896–908.
Winchester, V., 2023. Lichenometric dating and its limitations and problems: a guide for practitioners. Land 12, 611.
Worni, R., Huggel, C., Clague, J.J., Schaub, Y., Stoffel, M., 2014. Coupling glacial lake impact, dam breach, and flood processes: a modeling perspective. Geomorphology 224, 161–176.
Wright, H.E., Mann, D., Glaser, P., 1984. Piston corers for peat and lake sediments. Ecology 65, 657–659.
Zekollari, H., Huss, M., Farinotti, D., 2020. On the imbalance and response time of glaciers in the European Alps. Geophys. Res. Lett. 47.